

NASA TMX 55407

# RECENT MEASUREMENT OF THE MAGNETIC FIELD IN THE OUTER MAGNETOSPHERE AND BOUNDARY REGIONS

GPO PRICE \$ \_\_\_\_\_

CFSTI PRICE(S) \$ \_\_\_\_\_

Hard copy (HC) \$300Microfiche (MF) 150-

# 653 July 65

BY

J. P. HEPPNER

FACILITY FORM 602

N66-19498

(ACCESSION NUMBER)

59

(PAGES)

TMX 55407

(NASA CR OR TMX OR AD NUMBER)

(THRU)

1

(CODE)

30

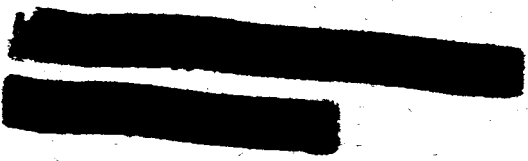
(CATEGORY)

NOVEMBER 1965

NASA

— GODDARD SPACE FLIGHT CENTER —  
GREENBELT, MARYLAND

(Presentation at the ESRO Colloquium on Auroral and Associated  
Magnetospheric Phenomena at Very High Latitudes, Stockholm,  
Sweden, November 16-18, 1965)




Recent Measurements of the Magnetic Field in the  
Outer Magnetosphere and Boundary Regions

by

J. P. Heppner

November 1965

(Presentation at the ESRO Colloquium on Auroral and Associated Magnetospheric  
Phenomena at Very High Latitudes, Stockholm, Sweden, November 16-18, 1965)



### Abstract

Within the framework of a brief review of recent magnetic field measurements in space, attention is directed to initial findings from the EGO-1 (OGO-A) satellite. Two particularly important results are: (1) circularly polarized, coherent oscillations of large amplitude are found at the bow shock front discontinuity. Study of the characteristics of these oscillations should significantly advance the understanding of collisionless shock waves, and (2) during periods of general magnetic disturbance when the magnetospheric tail field intensity is high, temporary decreases in tail field intensity are found to follow the onset of auroral zone negative bays in the same local time sector. This suggests that during the peak auroral activity which accompanies the onset of negative bays, the tail field in the bay sector partially collapses, or relaxes, from its highly stressed state.

An abnormal distortion of the outer magnetosphere on the day side of the earth coincides with the occurrence of an auroral zone positive bay near the same meridian. These correlations make it evident that a common mechanism is responsible for major changes in the outer magnetospheric field and the magnetic bays accompanying aurora.

## 1. Introduction

This paper takes advantage of a statement in the ESRO colloquium announcement that speakers assigned topics should feel free to model their presentations according to their best judgment, with the general idea of the symposium in mind. The "best judgment" exercised here is that the participants are familiar with existing publications on magnetic fields in space and would prefer to hear of several new results. Thus a disproportionate emphasis is placed on recent EGO (OGO-A) magnetic field measurements. The study and interpretation of these measurements is in an early stage. Initial findings rather than final results are thus given (See footnote\*). This information is presented relative to the framework of earlier experiments. The framework thus provides the review aspect of this presentation.

The primary concern for this colloquium is with the outer magnetosphere, the magnetospheric boundary, the transition region, and the bow shock front formed with the interplanetary medium. From theoretical studies and satellites such as Explorer's 10, 12, 14 and IMP-1 the earth's magnetic field in the noon-midnight plane is commonly depicted as shown in Figure I. The satellite magnetic measurements for this picture exist only at low to middle latitudes. The more recent satellites such as IMP's 2 and 3 and EGO have similar ( $\sim 30^\circ$ ) orbital inclinations, with the exception that EGO's inclination is positive (northern hemisphere apogee) rather than negative (southern hemisphere apogee).

---

\*A more comprehensive account of initial EGO findings is being prepared for journal publication by J. P. Heppner, B. G. Ledley, T. L. Skillman, M. Campbell, and M. Sugiura whose efforts are responsible for the EGO results reported here.

In considering the outer regions of the earth's field we must first recognize that the earth is imbedded in an interplanetary field of solar origin. The magnitude of this field has now been measured by several satellites and is found to usually be in the range 1 to 10 gammas with a mean near 5 gammas [1, 2, 3, 4]. The direction of the interplanetary field is found to be much more variable than the magnitude. However, when statistically averaged the dominant direction in the ecliptic plane, as shown in Figure 2 for IMP-1 measurements, is found to be in good agreement with the "garden hose angle" expected for lines of force being drawn away from the sun by a radial plasma flow. Using the same model, there does not appear to be an obvious explanation for the field being directed predominantly below the ecliptic plane as indicated in Figure 2. This suggests a need for longer periods of measurement in interplanetary regions and/or some improvement in existing theory. One of the most significant features found by Wilcox and Ness [3] in the analysis of field directions given by IMP-1 was that through three solar rotations the directions to and from the sun fell into a systematic pattern such that the interplanetary field could be divided into sectors of solar longitude, as shown in Figure 3. Within each sector a systematic behavior of field magnitude and solar wind flux was also apparent.

From studies of the solar-interplanetary field we thus have a picture that the earth's magnetic field is imbedded in a partially organized interplanetary field that co-rotates with the sun in response to the solar wind.

## 2. Boundary Locations

The location of the magnetosphere boundary from the noon hour back to the early morning hours is illustrated by the IMP-1 crossings shown in Figure 4. The positions are in good agreement with the earlier measurements of Explorer's 12 and 14 [5, 6]. Proceeding to larger solar angles there is also reasonable agreement with the multiple boundary crossings of Explorer 10 [7] that occurred on the evening side of the earth in 1961. For this illustration the Explorer 10 trajectory has been rotated about the sun-earth line (i.e.,  $X_{se}$  axis) in solar-ecliptic coordinates. The term "rectified" boundary crossings means that radial distances have been spherically rotated along meridian planes into the solar-ecliptic plane and that a small correction has been applied to account for the different magnetic latitudes of the sub-solar point.

IMP-1 [1] with a  $31.7 R_e$  apogee was also able to detect the bow shock front whose existence had been postulated in various theoretical studies on the basis that the solar wind velocity greatly exceeds the Alfvén velocity and that use of the Alfvén Mach number makes the geometry analogous to that of a neutral gas shock wave in supersonic flow. The success of this procedure is illustrated by the calculated curves of Spreiter and Jones [8] shown in Figure 4. The original calculated curves have been rotated by 5 degrees in Figure 4 to take into account the earth's orbital motion.

Several characteristic features of the magnetic field observed by a satellite in passing from the magnetosphere to the interplanetary medium are illustrated by Figure 5. The points shown are 5.46 minute averages

from IMP-1 along an orbit near the sunrise meridian. At the magnetosphere boundary ( $13.6 R_e$ ) there is a sharp change in both the field magnitude and direction. The variability of the field in the transition region is indicated by the standard deviations ( $\delta X_{se}$ ,  $\delta Y_{se}$ ,  $\delta Z_{se}$ ) of the 12 measurements taken for each component during each 5.46 minute interval. The sudden decrease in the standard deviations at  $19.7 R_e$  represents the shock front crossing into the weaker and more stable interplanetary field.

Figure 6 shows locations of a number of magnetosphere boundary crossings taken from EGO data on the afternoon side of the sub-solar point. The scatter of these positions is similar to that shown in Figure 4 for IMP-1 data but the average distance from the Spreiter and Jones [8] calculated curve is somewhat greater. A correction for the magnetic latitude of the sub-solar point has not been applied. This correction would decrease some of the distances by roughly 10 percent but there would still be some difference in the average distance relative to Figure 4. To determine whether this difference does or does not indicate a slight asymmetry of the geomagnetic cavity in addition to the 5 degree asymmetry attributable to the earth's orbital motion, a detailed comparison of relative solar wind parameters is required.

The shock front locations shown in Figure 6 also indicate an average distance from the earth slightly greater than the distances found for the morning hours shown in Figure 4. However, the stand-off distance (i.e., the separation of the magnetosphere boundary and the shock front) in Figure 6 appears to be in reasonable agreement with the stand-off distance

given by the calculated curves. Inasmuch as the stand-off distance at high Mach numbers is relatively insensitive to the Mach number this is an expected result.

### 3. Shock Front Characteristics

One of the most obvious features of the shock front in the afternoon sector shown in Figure 6 is that it appears to be frequently in motion. Thus when the satellite is approaching apogee, where its radial velocity relative to the earth is low, it finds itself alternately inside and outside the transition region as the shock front sweeps back and forth across the satellite trajectory. The minimum number of shock front crossings for small sections of a number of orbits is indicated beside each section in Figure 6 (e.g., 20 accompanying one of the long sections). The number indicated is a minimum because multiple crossings occurring within several minutes have been counted as one.

The locations shown in Figure 6 come from an incomplete sampling of two months of EGO data. As EGO is still working 14 months after launch there will be literally hundreds of shock front crossings available for detailed study. Hopefully these studies will reveal some of the basic properties of collisionless shock waves and thus direct attention to the most relevant of the many and diverse theories which have been put forth to explain collisionless shocks.

To aid in understanding the examples below the brief explanation of the EGO measurements given in Appendix (A) should be consulted.



Figure 7 illustrates a shock front crossing occurring when the spacecraft was in the 1 Kbit data mode. At approximately  $16^h 18^m 00^s$  there is a definite discontinuity in the field (indicated most clearly by the insensitive Z readings) that identifies the shock front. Near this point it is obvious that there are large amplitude rapid field oscillations superimposed on the 12 second spin modulation. These oscillations are also observed before and after  $16^h 18^m$  in the transition and interplanetary regions, respectively, but occur less frequently and with smaller amplitude as time increases or decreases from  $16^h 18^m$ . It is reasonable to assume that this also means decreasing amplitude with increasing distance from the shock front. The sampling rate on the sensitive scale is 2 measurements every 1.1 seconds and detailed examination shows that over limited periods of time, such as 5 seconds, alternate measurements represent peaks and troughs in the oscillation. This suggests that the principal oscillation is near a frequency of 1 cps or a harmonically related frequency.

The oscillation structure is considerably more clear when the satellite is in the 8 Kbit data mode with 14 readings per second as illustrated for a different shock front in Figure 8. In this case the crossing is from an interplanetary field to a transition region field but again one sees decreasing amplitude progressing both ways from the front which occurs near  $00^h 02^m 10^s$ . The principal oscillation frequency in this crossing varies between 0.8 and 1.2 cps. Between 1.2 and 1.5 cps the power spectra of this sample shows an abrupt decrease of almost a factor of 10. Taking 1 cps as a representative frequency: this frequency is at least two orders

of magnitude too low to be either the electron or proton plasma frequency, it is much lower than the electron cyclotron frequency, and is at least a factor of 6 too large to be the ion cyclotron frequency. The closest unique frequency is the lower hybrid resonance frequency but for an exact fit this requires a field of  $1.5\gamma$  which does not correspond to the observed field.

When the oscillation is large, such as near  $00^h 02^m 15^s$  in Figure 8, it is also apparent on the insensitive X-axis as shown in Figure 9. The 90 degree phase displacement from the Y axis and the lack of amplitude dependence on position in the 12 second spin cycle tells one that the oscillation is essentially circularly polarized.

The frequency and polarization characteristics thus suggest that any propagation of this wave would occur in the same general regime as the whistler mode. However, caution must be exercised until a large number of crossings have been analyzed. Doppler shifts could be acting in a manner that would affect both the designation of frequency and the sense of the polarization. Also to illustrate that the examples above do not represent a complete picture, a third shock crossing is illustrated in the raw machine plots of Figures 10 and 11.

Figure 10 shows 30 seconds of Y and Z axis data taken immediately following a shock front crossing from interplanetary to transition region fields. The frequency of the prominent oscillation apparent in the Y readings is close to 0.8 cps and thus is similar to the examples previously

given. However, when we look at the 30 seconds immediately preceding the 30 seconds shown in Figure 10, the oscillatory field behavior on the interplanetary side of the front is remarkably different, as shown in Figure 11. It is apparent that much higher frequencies than those resolved by 14 samples/sec are present. It is also apparent that the occurrence of high frequencies is related to the presence of the shock front in that proceeding back in time an additional one minute (not shown) one finds a quiet interplanetary field in which the Y axis data forms a smooth sine wave with virtually no scatter of the points such as the scatter in Figure 11. This suggests a highly effective damping mechanism.

#### 4. The Transition Region

In working with EGO data it has become obvious that fields in the transition region show remarkably different characteristics at different times. We are presently trying to find some simple means of characterizing the different types of behavior to see what may be causing these differences and to see what relationship each type of behavior may have with other phenomena. A crude classification shows at least four types of behavior:

- (1) irregular, short period fluctuations superimposed on a general field. The amplitude can vary greatly but is often small.

The transition region fields shown in Figures 7 and 8, in the sections remote from the shock front, would fall in this category.

- (2) periods of slowly varying fields
- (3) periods when the field appears to be highly stable for many minutes and even hours, and
- (4) periods when the field appears to be completely chaotic, or turbulent.

It is anticipated that correlations with the different types of behavior may prove important to understanding the transfer of energy to the magnetosphere.

#### 5. The Magnetospheric Boundary

Numerous examples of the change in magnetic field direction and/or magnitude in crossing between magnetospheric and transition region fields have appeared in the analyses of Explorer's 10, 12, 14 and IMP-1 [1, 5, 6, 7]. These will not be discussed in detail here. It should, however, be noted that some of the EGO magnetospheric boundary crossings show a feature that has apparently been missed or neglected in previous analyses. The observation is that for periods such as 20 seconds to 2 minutes prior to encountering a true discontinuity the field direction, in some cases, deviates significantly but in a steady manner without any sharp changes or appearance of typical transition region fluctuations. In these cases it may be more correct to speak of a thin boundary layer. Deviations in this layer have been observed in both the same and opposite directions as the normal field bending resulting from the solar wind compression. This is indicated in the pictorial representation of Figure 12.

#### 6. Long Period Magnetospheric Field Oscillations

Characteristics of long period oscillations within the magnetosphere observed by Explorer's 12 and 14 have been presented by Patel [9]. It appears clear that these are hydromagnetic waves. It is apparent in the EGO data that quasi-periodic, large amplitude, oscillations with periods in the range 4 to 15 minutes occur frequently in the outer magnetosphere.

As indicated pictorially in Figure 12 there also is a tendency for these oscillations to appear most frequently in the outermost regions of the magnetosphere. Whether this is a consequence of the amount of time the satellite spends in the outer magnetosphere as opposed to the time in regions nearer the earth needs to be resolved. These oscillations are also frequently observed in the magnetospheric tail. (Note: the illustration of both a thin boundary layer and long period oscillations in Figure 12 does not imply that these two features are related).

#### 7. The Magnetospheric Tail

The geomagnetic tail field at low latitudes has been extensively mapped in the southern hemisphere by Explorer 14 [10] and IMP-1 [1] and data in the northern hemisphere is being obtained from EGO. Figure 13 illustrates the characteristic anti-solar field direction projected onto the ecliptic plane from different distances ( $Z_{se}$  in earth radii) below the plane. Sometime after 1961 when this field was first measured to  $40 R_e$  by Explorer 10 [7], energetic radiation was found near the equatorial plane in the tail region. Several investigators [11, 12, 13] noted the implications of these observations and concluded that there should be an equatorial surface in the tail in which the field direction would reverse rather abruptly from this anti-solar direction to the opposite (i.e., solar) direction in the northern hemisphere. This is often referred to as a "neutral sheet" discontinuity. The IMP measurements [14] subsequently revealed the existence of the field reversal region. Figure 14 illustrates these reversals in solar-ecliptic coordinates.

Following the IMP-1 findings a second look at Explorer 14 data brought forth the dramatic example of field reversal shown in Figure 15. More generally, however, the Explorer 14 data, at distances 8 to 15  $R_E$ , showed a transition from anti-solar to solar directed fields more like that of Figure 16. That is, a region of low field magnitude rather than a sharp transition separated the hemispheres of anti-solar and solar directed fields. Cahill [10] used the term "magnetospheric inflation" to describe this behavior. Although time will not permit a discussion here of the uncertainties in the shape of the inflated region and postulated "neutral sheet" configurations, the available data suggests: (a) that there is probably latitudinal narrowing of the field reversal region with increasing distance from the earth such that the term "neutral sheet" becomes more realistic at great distances, and (b) that the location of the field reversal region is related to both the geomagnetic equator and the latitude of the sub-solar point in a manner in which the anti-solar direction becomes more important with increasing distance.

During disturbed magnetic conditions (i.e.,  $K_p$  indices are large and there is appreciable  $D_{st}$  variation at low latitudes) IMP-1 [15] and Explorer 14 [10] results show that the average magnitude of the tail field is significantly increased at latitudes remote from the field reversal region. The increase in average field intensity, relative to quiet periods, is observed both in the initial and main phase stages of a magnetic storm [15].

#### 8. The Magnetospheric Tail (EGO measurements)

As described in Appendix (A), two sensors measure the field in the XY plane of the EGO spacecraft and one sensor measures the field along the

spacecraft Z axis which is also the spin axis. To obtain a complete vector representation a reference direction is needed in the XY plane during each 12 second spacecraft spin period. Although information exists to give this reference direction, the reduction on a systematic basis has been complicated and until complete confidence is established in the attitude data provided it appears wise to present data in a form not affected by attitude errors. Fortunately, the orientation of the satellite, as illustrated in Figure 17, is such that at large distances from the earth, and especially on inbound passes, the XY sensors are primarily measuring the field in a meridian plane of the earth and Z measures primarily the field normal to a meridian plane. Thus in a data presentation like Figure 18 the sign of the Z axis deviation tells one whether the field is directed toward or away from the sun.

Figure 18 is an inbound pass in the magnetospheric tail occurring during the decay phase of a moderate magnetic storm. It is selected for presentation here because it serves to illustrate a number of general features within a limited period of time. The large average magnitude of the tail field previously discussed is quite evident at distances  $>10 R_E$ . The sign of Z tells one that the field is directed toward the sun. (i.e., the satellite is in a northern hemisphere field although not far from the equatorial plane).

At distances of 4 to  $8 R_E$  the EGO orbit provides data which is unique in the sense that measurements are obtained at the equator on inbound passes. In Figure 18 it is apparent that the field magnitude in the

meridian plane in this region is considerably lower than the reference field (computed from Jensen and Cain coefficients). A first impression in noting this low magnitude region is to jump to the conclusion that it represents the  $D_{st}$  ring current location. However, as previously presented [16], it can be shown, through comparison of surface  $D_{st}$  variations with EGO data on successive orbits and in terms of relative magnitudes of the deviation at  $4 R_e$  with surface  $D_{st}$  values, that such a source does not adequately explain the surface disturbance. This also means that a current sheet located in a tail neutral surface does not account for the surface  $D_{st}$  variation. In Figure 18 it is apparent that the field deviation is decreasing rapidly between 5 and  $3.8 R_e$ . This trend, together with the inadequacy of sources beyond  $3.8 R_e$ , suggests that at least some fraction of the surface  $D_{st}$  variation comes from sources below  $3.8 R_e$ , probably in the 2 to  $3.5 R_e$  region (a review of the likelihood of a ring current in this region is given in [13]).

Although the measurements in Figure 18 were taken during the decay of a storm a low magnitude at the equator near  $6 R_e$  on the night side of the earth is observed under non-storm conditions as well. There are, however, cases under very quiet conditions in which the deviation from reference field values is very small. It should also be noted that the region is not confined to local times near midnight. The depressed field in Figure 19 near evening twilight illustrates this point. Although a disturbance had occurred earlier, values of  $K_p=1$  correspond to the interval shown. Figure 19 at  $R_e > 9$  also shows long period oscillations of the type discussed in Section 6., above.



9. Magnetospheric Field Behavior during Auroral Zone Magnetic Bays

The EGO measurements indicate a close relationship between magnetospheric field behavior and auroral zone magnetic bays. Potentially this association of behavior can be highly important in that it provides clues to the dynamical processes involved. Figure 18 again serves as an illustration. Near 19:37 and 21:39 UT the XY measurements (approximately in the meridian plane) show a relatively abrupt decrease superimposed on the otherwise high field level mentioned in the previous section. Looking at auroral zone surface observatories near the same local time zone one finds that about 14 minutes prior to each of these times there was an occurrence of the onset of a negative bay. In the case of the first bay there is also an abrupt recovery which ends at 20.31 UT at both the satellite and surface locations.

If we look just at Figure 18, two possible explanations come to mind: (1) that the magnetospheric tail is further stretched and/or inflated such that the equatorial low magnitude or "neutral sheet" region expands latitudinally to include the satellites location at the time of the bay, or (2) that the tail field tends to collapse back to a less stressed condition at the time of the bay such that the field intensity in the tail is decreased. These are directly opposite conditions and it is important to know which is correct. What we have done so far, to try to resolve this dilemma, is to look for examples in which the satellite is at a high enough latitude,  $>20^\circ$ , to make it improbable that the satellite could fall within the low magnitude, or neutral sheet, region. Two very clear, and

other marginal, cases have been found and in each case the behavior is essentially the same as in Figure 18 with differences appearing only in the number of minutes between the bay and satellite disturbance onset time<sup>u</sup> (Note: in one case the onset time was essentially simultaneous). Thus, at least until contradictory data appears, the view that is favored is that the tail field is partially collapsing back toward a less stressed condition during a negative bay. (Note: the number of examples has been small because a number of conditions must be satisfied to make the correlation; the most limiting is having a surface observatory near the same local time as the satellite and then having the onset of a negative bay originate near that observatory. As more auroral zone magnetograms become available additional correlations will be possible).

An outline to illustrate the role of negative bays is shown in Figure 20. Several items should be noted. The first is that the tail field decrease during a negative bay may be roughly confined to sectors of the tail related in local time to the region of negative bay occurrence (i.e., it has not been demonstrated that the entire tail field tends to collapse back). Second, the inferred transfer of energy does not represent the total energy of the disturbance. Third, there is no estimate of the degree to which energized particles from within the magnetosphere tend to inflate the magnetosphere in opposition to the magnetospheric compression by the solar wind.

Proceeding to the day side of the earth the importance of relationships between auroral zone bays and magnetospheric field behavior is again

apparent. Figures 21 and 22 show data on outbound passes taken 8 days apart on days of similar general magnetic activity but having specific differences at the actual time of the data. The period of the EGO orbit is such that precisely 3 orbits occur every 8 days; thus except for a  $1^\circ$  per day longitude shift the relative positions of the satellite and the Kiruna Observatory are the same every 8 days.

The measurements on October 4 (Figure 21) show a relatively normal field distortion for northern latitudes in the afternoon, pre-twilight, time sector. The increased magnitude, relative to the reference field, is expected from solar wind compression of the field. The sign of Z, relative to the reference field, is negative at large distances as expected if the magnetic meridian plane is bent in the anti-solar direction by the compression (Note: to recognize this point rotate the orbit and satellite orientation shown in Figure 17 to the appropriate local time. The +Z axis is then roughly anti-solar). At the time of these measurements there is a lull between bay disturbances in the auroral zone, as shown in Figure 21 by Kiruna near the satellites local time and College on the night side.

The EGO measurements on October 12 (Figure 22) have a markedly different appearance. Throughout this data interval there was bay activity on the night side (College magnetogram). At 11:30 UT positive bay activity began in the afternoon (Kiruna magnetogram) (Note: identification of 11:30 UT as the start time comes from looking at all three components at Kiruna and not just the H trace shown in Figure 22). At 11:41 UT near  $4.5 R_e$  ( $L \approx 5.5$ ) the satellite measurements show the beginning of a

disturbance but one cannot be sure whether the important parameter here is the time or the change in L shell. A field decrease is first observed but with increasing distance the dominant feature becomes a distortion of the field direction which is the opposite of the normal distortion. Considering only the distortion of the magnetic meridian plane the bending of the meridian plane is in the solar direction as illustrated in Figure 23.

To explain the abnormal distortion associated with the positive bay of October 12 there is some appeal in imagining that a region of energetic magnetospheric plasma on the night side pushes into the day side in the form of a "tongue" to stress the magnetic meridian in opposition to the solar wind stress. Such a picture may not, however, represent reality. A second and more detailed comparison of October 4 and October 12 suggests that a reasonable model could be constructed by having electric currents flow along field lines. The complete circuit might then involve the eastward electrojet current.

In closing, I believe it is appropriate relative to the other topics of this colloquium to note the importance of studying auroral zone magnetic bay phenomena and to note also that the electric fields which we commonly associate with auroral electrojets are probably an important element in the dynamics of the magnetosphere. Hopefully several years hence we will be able to speak of joint electric and magnetic field measurements in discussing convective, and other, processes. Similar considerations of joint electric and magnetic field measurements apply to understanding the shock wave structures emphasized in this presentation.

## Appendix (A)

### A Brief Explanation of OGO-A (EGO-1)

#### Magnetic Field Measurements

The OGO (EGO and POGO) spacecraft are designed to be stable spacecraft. However, two boom appendages on OGO-A (EGO-1) failed to deploy and this contributed to the failure of the stabilization system. One of the two booms that failed to deploy held the magnetometers. The net result was that: (a) the spacecraft assumed a spin stable configuration rather than complete stabilization, (b) the optical pumping, Rb-vapor, magnetometer was left against the spacecraft body in a high gradient field where it could not operate, and (c) the three-axis fluxgate magnetometer was left in a position several feet from the spacecraft body in a region of moderate spacecraft fields for this proximity.

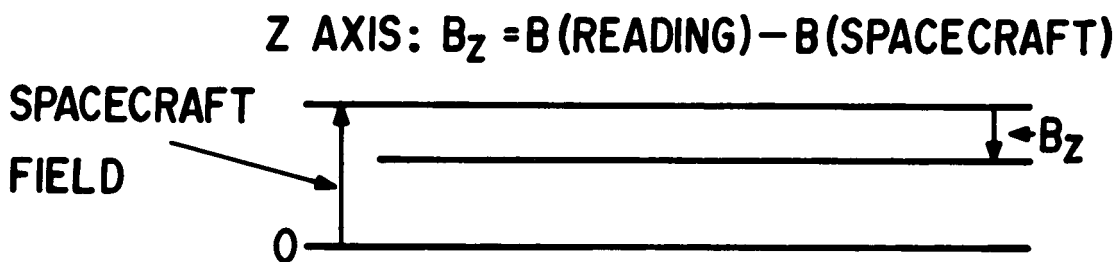
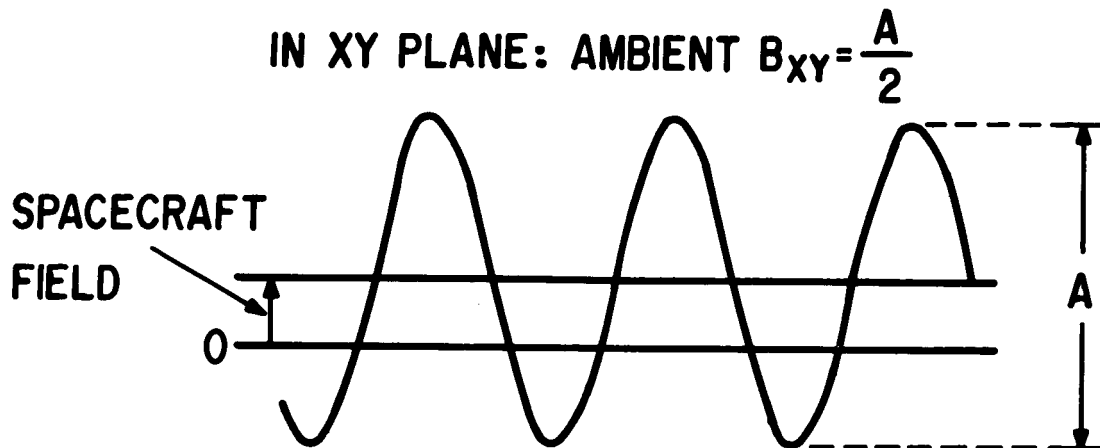
In the undeployed state the fluxgate axes are, however, coincident with the X, Y, Z body axes of the spacecraft such that the -Z and -Y instrument axes coincide, respectively, with the +Z and +Y spacecraft body axes and the +X instrument axis coincides with the +X spacecraft axis. The Z axis of the spacecraft is also the spin axis and the spin period is approximately 12 seconds. In this situation the X and Y sensors each measure the ambient magnetic field in the XY plane independent of the spacecraft field as illustrated in Figure A-1. The Z axis measurement is not, however, independent of the spacecraft field and the contribution of the spacecraft field must be deduced by other means. Fortunately, the spacecraft field has been exceptionally stable as shown by a long history of X and Y measurements and the Z spacecraft

field is thus determined to an estimated accuracy of  $\pm 2$  gammas (a value imposed by the insensitive scale resolution as explained below) by examining the Z measurements over many long periods in interplanetary regions.

As illustrated in Figure A-1 the spacecraft field is equivalent to having a shift in the fluxgate zero level. The EGO-1 field is such that this shift is  $-9^\gamma$  along the Y instrument axis,  $-59^\gamma$  along the X instrument axis, and  $-54^\gamma$  along the Z instrument axis. As the instrument has two ranges of sensitivity, see Figure A-1, this has the additional consequence in weak fields that highly sensitive readings (i.e.,  $0.24^\gamma$ ) are obtained only from the Y sensor in the XY plane. The X and Z sensors are limited to readings within digital steps of 3 to  $4^\gamma$  (i.e.  $\pm 1.5$  to  $2^\gamma$ ).

Figure A-1 also shows the sampling rate relative to the 12 second spin period for each of the three data modes provided by the spacecraft. In readings per second for each axes the rates are: 1.8 measurements per second in the 1 Kbit mode, 14 measurements per second in the 8 Kbit mode, and 114 measurements per second in the 64 Kbit mode on the sensitive scale and one-half this rate on the insensitive scale.

The instrument response to oscillating fields is flat to 10 cps with an approximate exponential drop-off at higher frequencies such that the response is close to 50 percent at 50 cps. Peak-to-peak instrument noise levels are  $\pm 0.12$  gammas.



	<u>SENSITIVE SCALE</u>	<u>INSENSITIVE SCALE</u>
NOMINAL FIELD RANGE	$\pm 30^\gamma$	$\pm 500^\gamma$
DIGITAL RESOLUTION	$0.24^\gamma$	$3.5^\gamma$

#### READINGS PER SPIN PERIOD PER AXIS

<u>DATA MODE</u>	<u>SENSITIVE</u>	<u>INSENSITIVE</u>
1 KILOBIT	20.5	10.3
8 KILOBIT	165	83
64 KILOBIT	1322	661

Figure A-1

## References

1. Ness, N. F., Searce, C. S., Seek, J. B., and Wilcox, J. M., A summary of results from the IMP-1 magnetic field experiment; Presented at COSPAR, May 1965; to be published in Space Research VI.
2. Greenstadt, E. W., Final estimates of the interplanetary magnetic field at 1 AU from measurements made by Pioneer V in March and April 1960; TRW Systems Report 9890-6001-RU001, September 1965.
3. Wilcox, J. M. and Ness, N. F., A quasi-stationary co-rotating structure in the interplanetary medium, J. Geophys. Res. (to be published), NASA-GSFC preprint X-612-65-302.
4. Coleman, P. J., Jr., Smith, E. J., Davis, L., Jr., and Jones, D. E., paper presented at COSPAR, May 1965; to be published in Space Research VI.
5. Cahill, L. J. and Amazeen, P. G., The boundary of the geomagnetic field, J. Geophys. Res., 68, 1835 (1963).
6. Cahill, L. J., The Geomagnetic Field, Chapter 9, Space Physics, ed. by D. P. LeGalley and A. Rosen, John Wiley and Sons, Inc., (1964).
7. Heppner, J. P., Ness, N. F., Searce, C. S., and Skillman, T. L., Explorer 10 magnetic field measurements, J. Geophys. Res., 68, 1 (1963).
8. Spreiter, J. R. and Jones, W. P., On the effect of a weak interplanetary magnetic field, J. Geophys. Res., 68, 3555 (1963).
9. Patel, V. L., Long period hydromagnetic waves in the magnetosphere: Explorer 14; presented at COSPAR, May 1965; to be published in Space Research VI.



10. Cahill, L. J., Jr., Inflation of the magnetosphere near 8 earth radii in the dark hemisphere; presented at COSPAR, May 1965; to be published in Space Research VI.
11. Axford, W. I., Petschek, H. E., and Siscoe, G. L., The tail of the magnetosphere, J. Geophys. Res., 70, 1231 (1965).
12. Dessler, A. J. and Juday, R. D., Configuration of auroral radiation in space, Planet. and Sp. Sci., 13, 63 (1965).
13. Heppner, J. P., Satellite and Rocket Observations, (July 1964), Chapter V-2, Physics of Geomagnetic Phenomena, ed. by S. Matsushita and W. H. Campbell, Academic Press, Inc. (to be published).
14. Ness, N. F., The earth's magnetic tail, J. Geophys. Res., 70, 2989 (1965).
15. Behannon, K. W. and Ness, N. F., Magnetic storms in the earth's magnetic tail, NASA-GSFC preprint X-612-65-417, October 1965.
16. Heppner, J. P., Campbell, M., Skillman, T. L., and Ledley, B. G., Preliminary report on EGO magnetic field measurements, Amer. Geophys. Union, Annual Meeting, April 1965.

### Figure Captions

1. A pictorial illustration of the geomagnetic cavity in the noon-midnight meridian plane.
2. Statistical distribution of interplanetary field directions in solar-ecliptic coordinates during 3 solar rotations, from IMP-1 [Wilcox and Ness, 3].
3. Sector structure of the interplanetary magnetic field suggested by IMP-1 measurements. A + sign designates fields directed away from the sun; a - sign designates fields directed toward the sun. From averages over 3 hour intervals for 3 solar rotations [Wilcox and Ness, 3].
4. Locations of the magnetopause and rectified shock wave at pre-noon local times from IMP-1, compared with computed boundaries of Spreiter and Jones [8] in solar-ecliptic coordinates (axes  $X_{se}$ ,  $Y_{se}$  lie in the ecliptic plane) [Ness, et al., 1].
5. Magnetic field measurements from IMP-1 on January 5, 1964 near the sunrise meridian [Ness, et al., 1].
6. Magnetospheric boundary and shock front locations at afternoon local times from EGO, compared with computed boundaries of Spreiter and Jones [8] in solar-ecliptic coordinates.
7. Magnetic field measurements during a bow shock front crossing with the EGO spacecraft in the 1 Kbit data mode (See Appendix A for explanation of sampling rate, etc.)

8. Magnetic field measurements during a bow shock front crossing with the EGO spacecraft in the 8 Kbit data mode (See Appendix A for explanation of sampling rate, etc.)
9. Expanded plot from the shock front crossing shown in Figure 8. The insensitive X axis is added to illustrate polarization of the oscillation.
10. Machine plot of raw data for the Y, sensitive (dots), and Z, insensitive (asterisks), channels between  $14^{\text{h}}00^{\text{m}}31^{\text{s}}$  and  $14^{\text{h}}01^{\text{m}}01^{\text{s}}$  on day 353, 1964. Full scale is 80 gammas. Spacecraft data mode is 8 Kbit. (See Appendix A for explanation of zero level, etc.)
11. Machine plot of raw data for the Y, sensitive (dots), and Z, insensitive (asterisks), channels for the 30 seconds,  $14^{\text{h}}00^{\text{m}}01^{\text{s}}$  to  $14^{\text{h}}00^{\text{m}}31^{\text{s}}$ , preceding the data shown in Figure 10. The principal shock front discontinuity is near  $14^{\text{h}}00^{\text{m}}25^{\text{s}}$ .
12. Pictorial illustration (See text for explanation).
13. Summary of the distortion of the geomagnetic field in the southern hemisphere tail region from IMP-1. Dashed lines give distances below the ecliptic plane in earth radii ( $Z_{\text{se}}$  coordinate). Vectors are from hourly average components  $X_{\text{se}}$  and  $Y_{\text{se}}$  in solar ecliptic coordinates [Ness, et al., 1].
14. Summary of hourly average components in the  $X_{\text{se}}$ ,  $Z_{\text{se}}$  plane for IMP-1 measurements in the northern ecliptic hemisphere for  $Y_{\text{se}}$  satellite coordinates  $\geq -3 R_{\text{e}}$ . Note field reversals [Ness, et al., 1].

15. Explorer 14 measurements on the night side of the earth. Vectors are projections of the magnetic field vector on the local magnetic meridian plane. End points of vectors are plotted at the geomagnetic latitude and radial distance of the measurement. The anti-solar direction is shown in geomagnetic latitude in the midnight meridian plane for times near satellite apogee [Cahill, 10].
16. Explorer 14 measurements on the night side of the earth. Vectors are plotted as in Figure 15 [Cahill, 10] .
17. Illustration of the EGO spin axis orientation in inertial coordinates relative to the spacecraft's location in orbit. Equatorial plane projection.
18. EGO magnetic field measurements on the night side of the earth for the inbound pass on September 28-29, 1964 and selected surface magnetic field records from auroral zone observatories.
19. EGO magnetic field measurements near the evening twilight sector for the inbound pass on November 23-24, 1964.
20. Outline to illustrate the associated role of negative bays in the behavior of the magnetospheric tail field.
21. EGO magnetic field measurements in an afternoon sector for the outbound pass on October 4, 1964 and selected surface magnetic field records from auroral zone observatories.
22. EGO magnetic field measurements in an afternoon sector for the outbound pass on October 12, 1964 and selected surface magnetic field records from auroral zone observatories.

23. Pictorial representation of the relative bending of the magnetic meridian plane at distances  $R_e > 6$  on October 4 and October 12, 1964.
- A-1. Illustration of parameters involved in EGO-1 (OGO-A) magnetic field measurements.

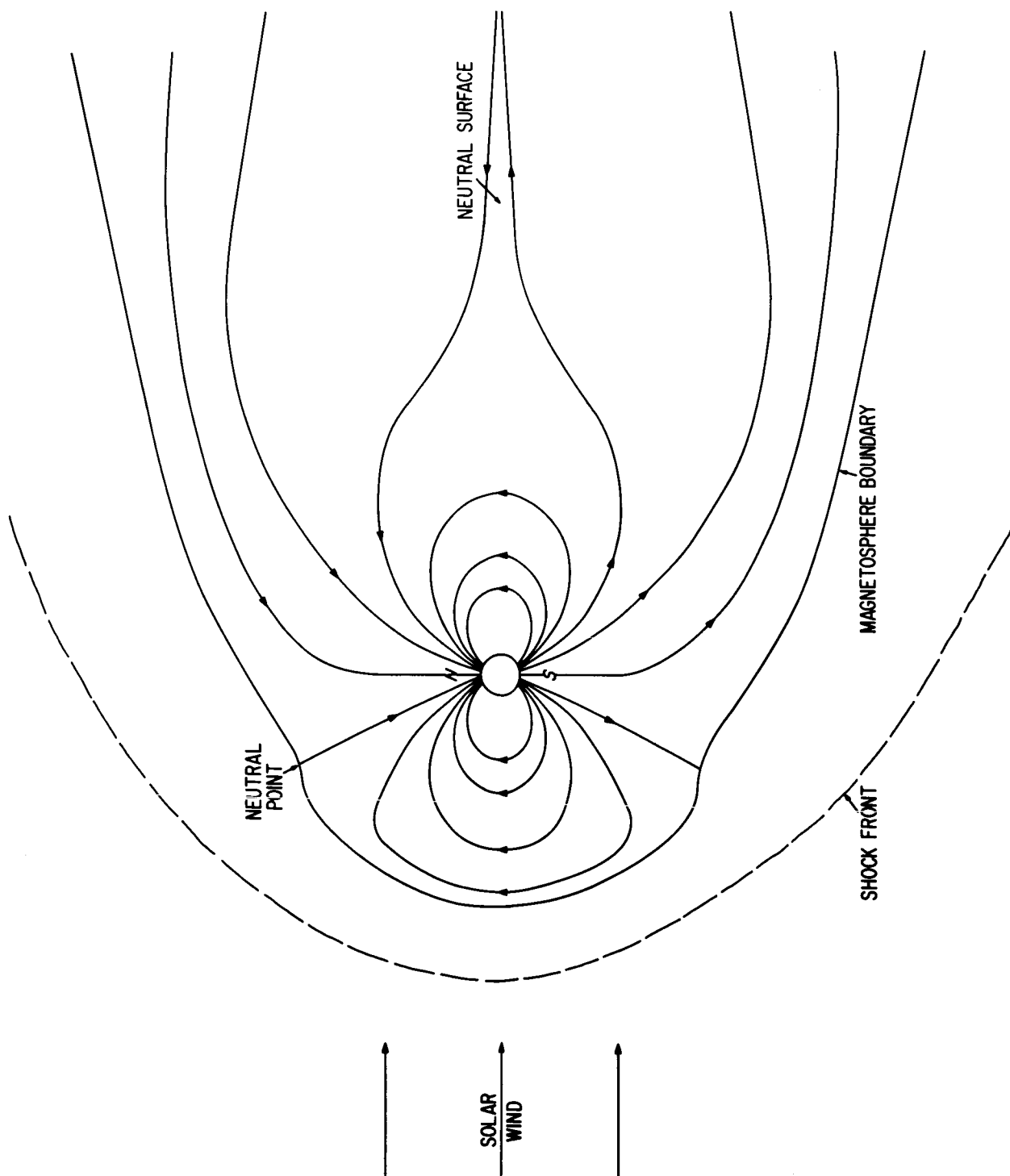
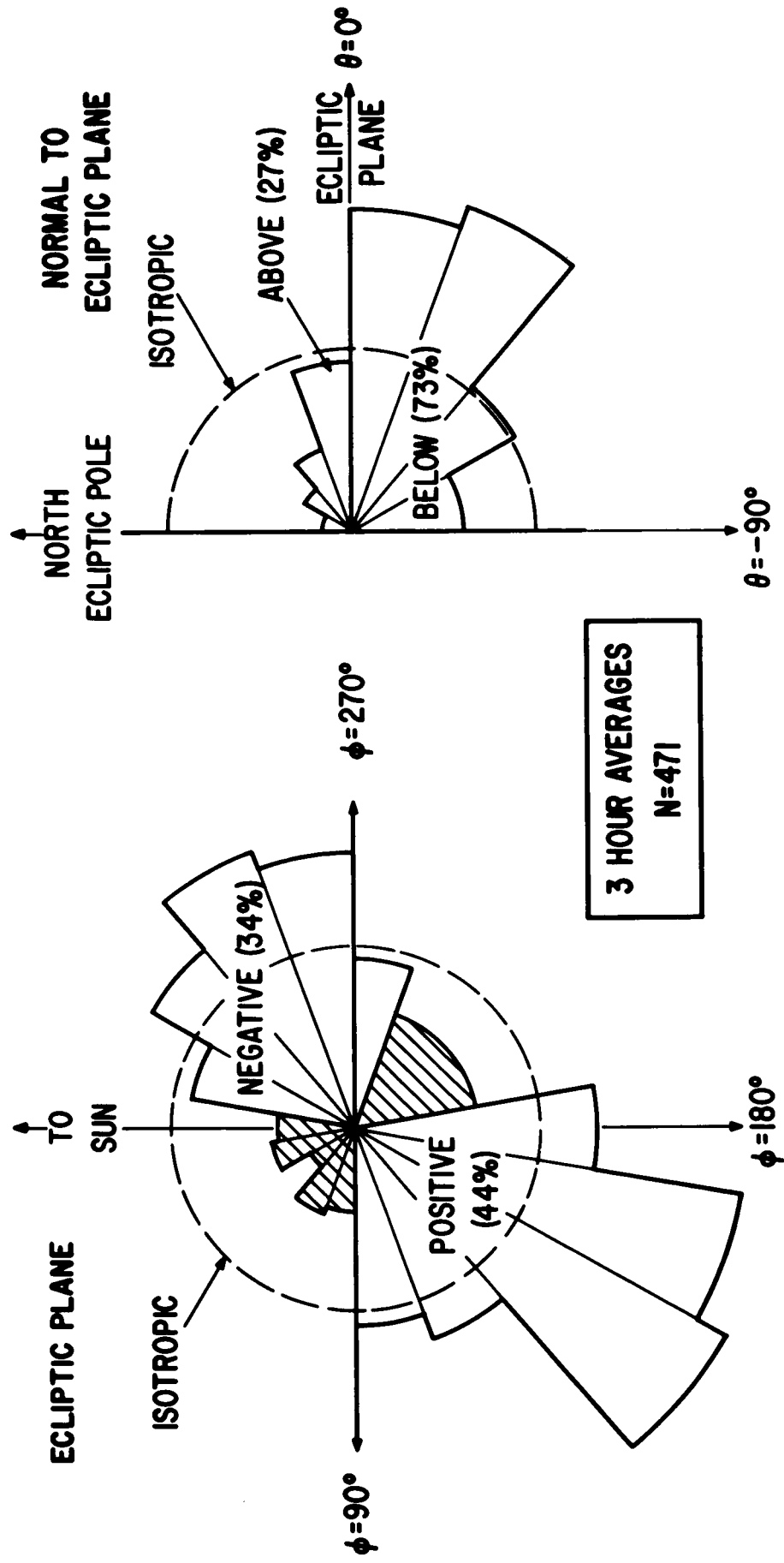


Figure 1



**DISTRIBUTION OF INTERPLANETARY MAGNETIC FIELD DIRECTION**

Figure 2

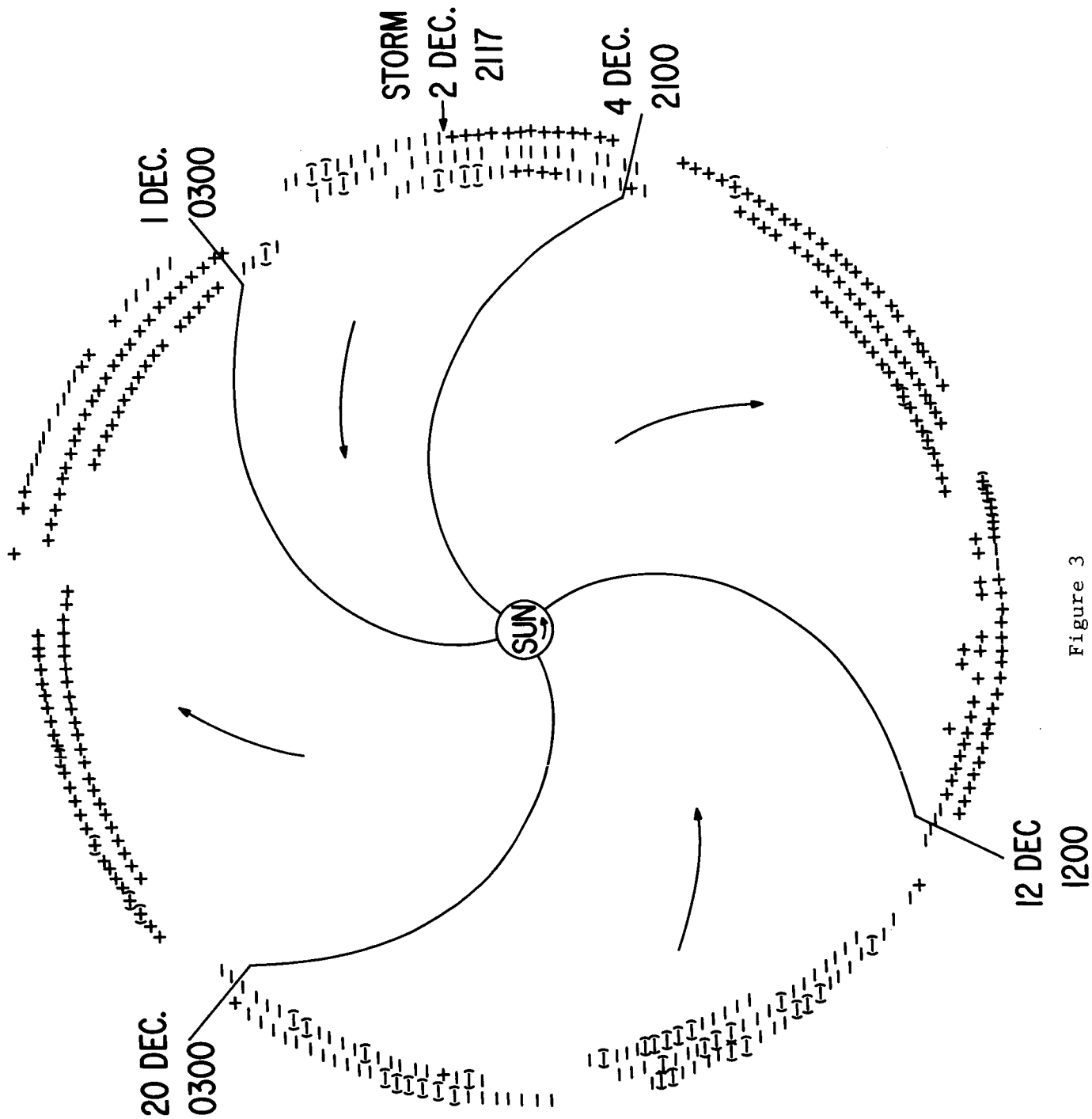


Figure 3



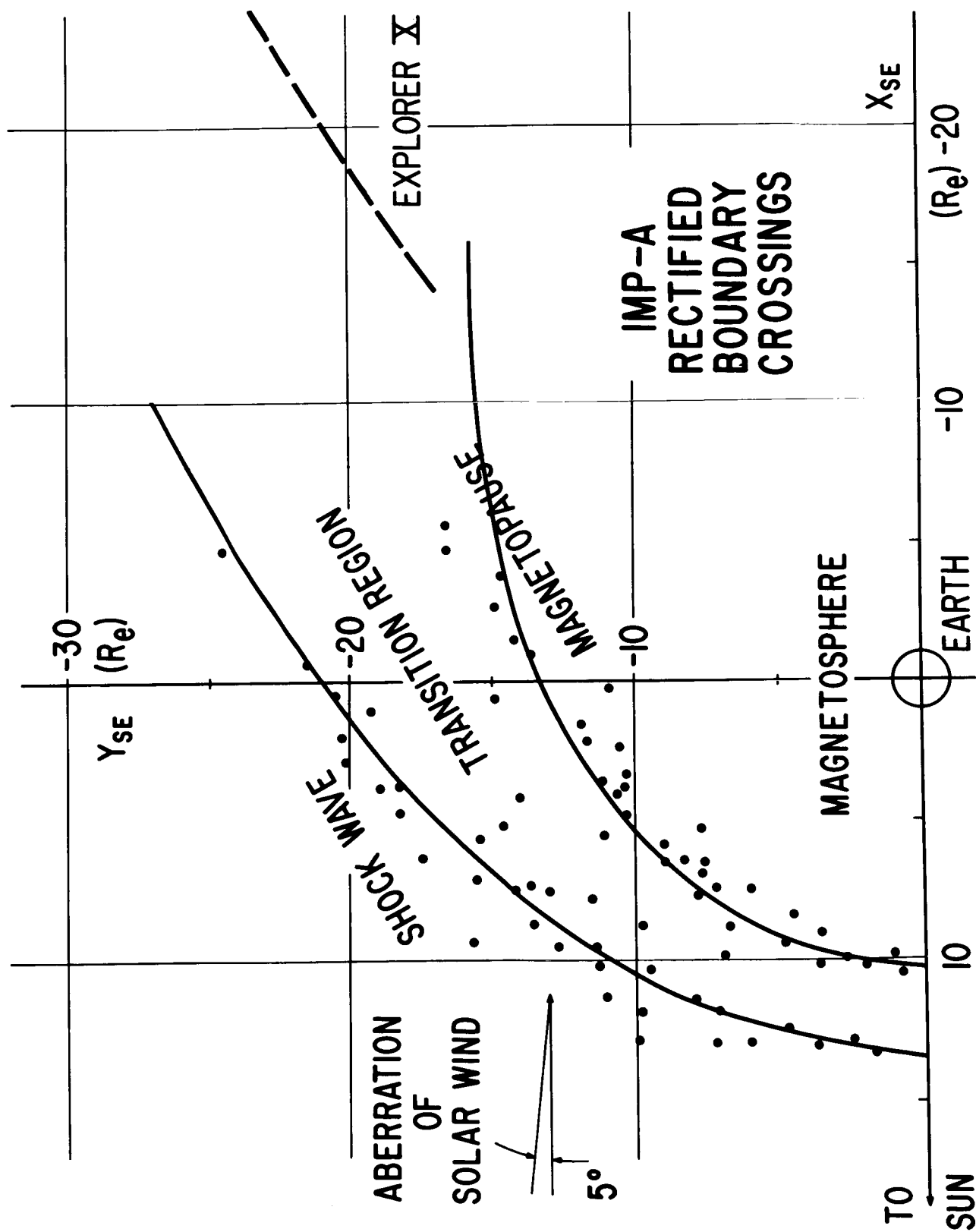


Figure 4

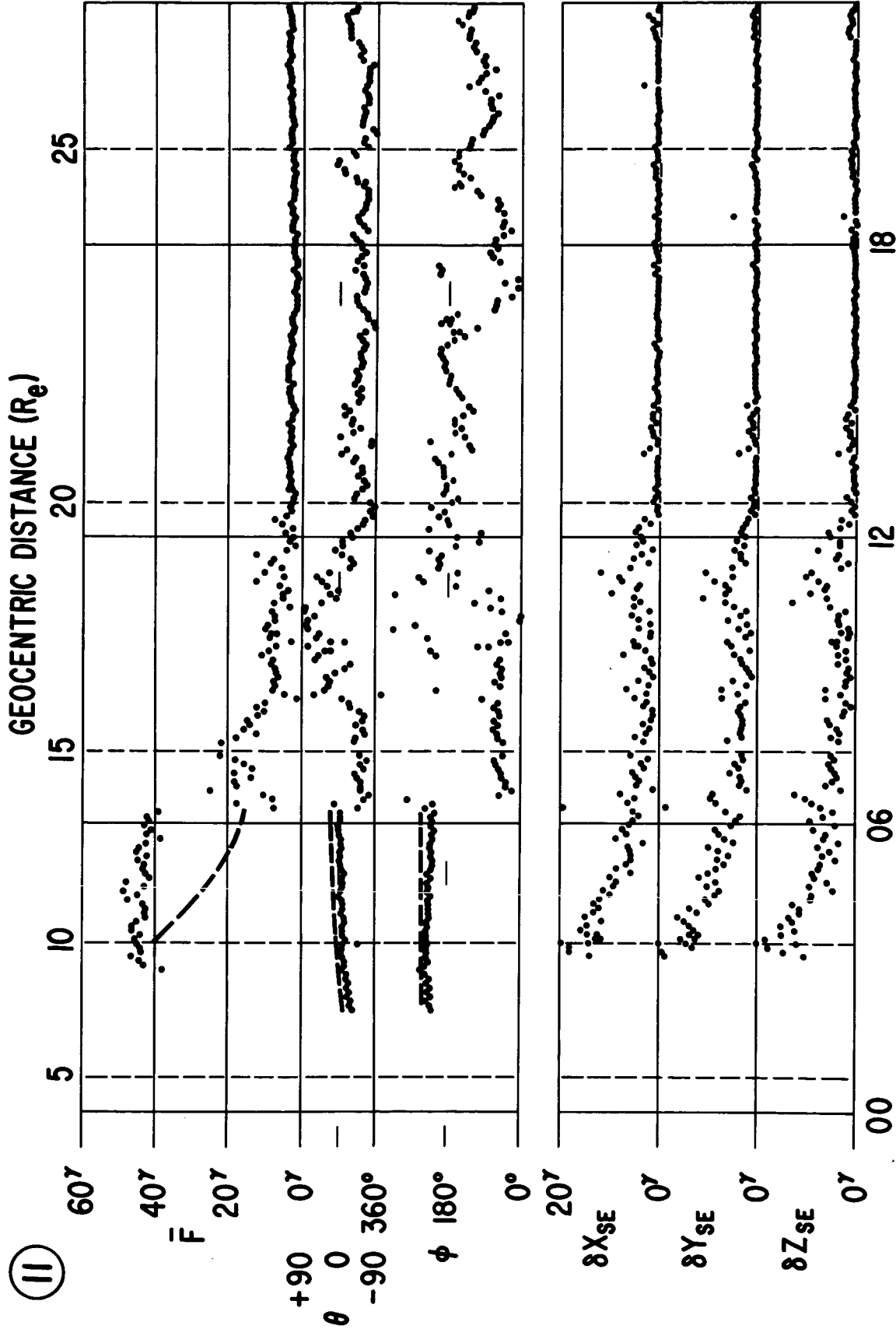


Figure 5

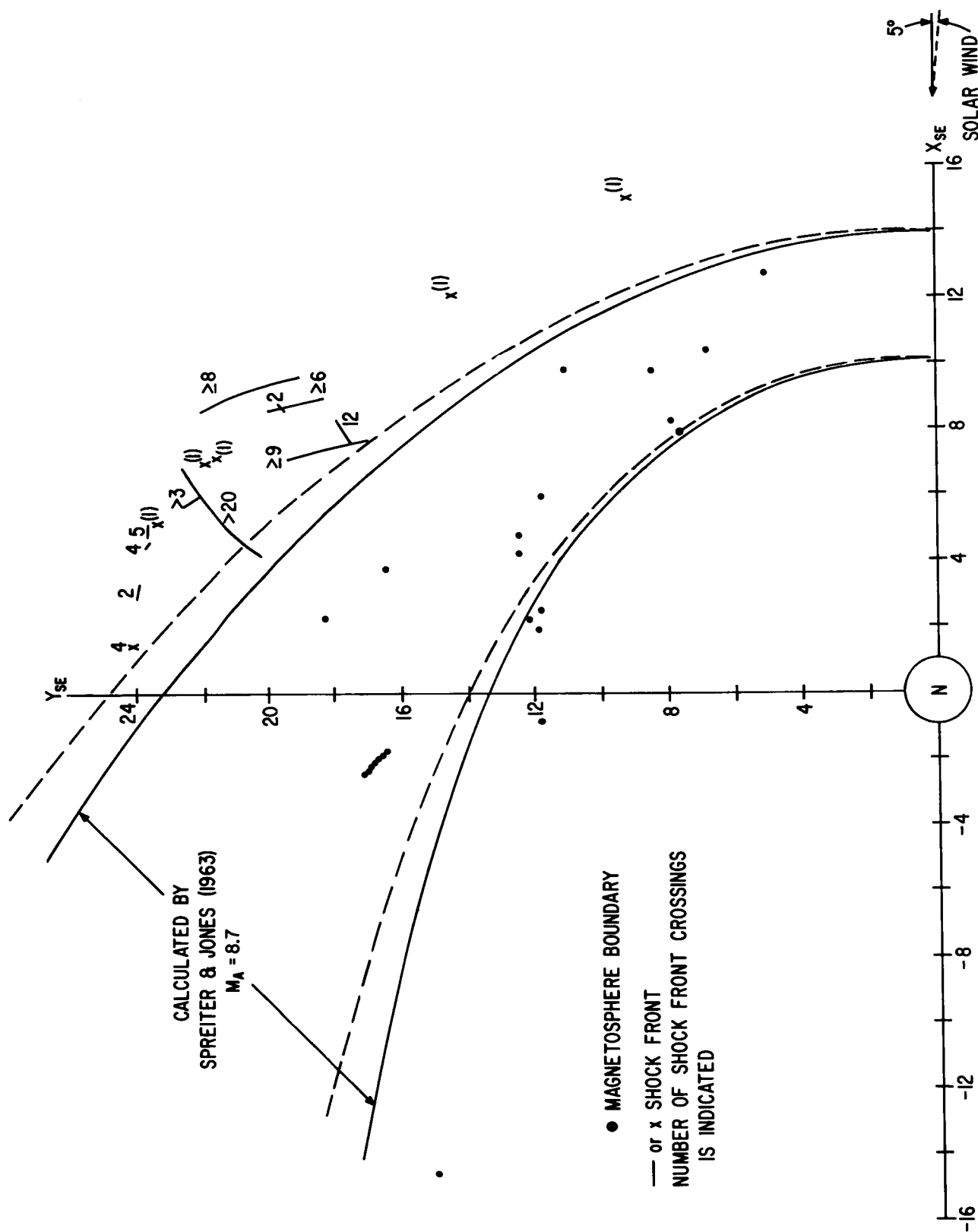


Figure 6

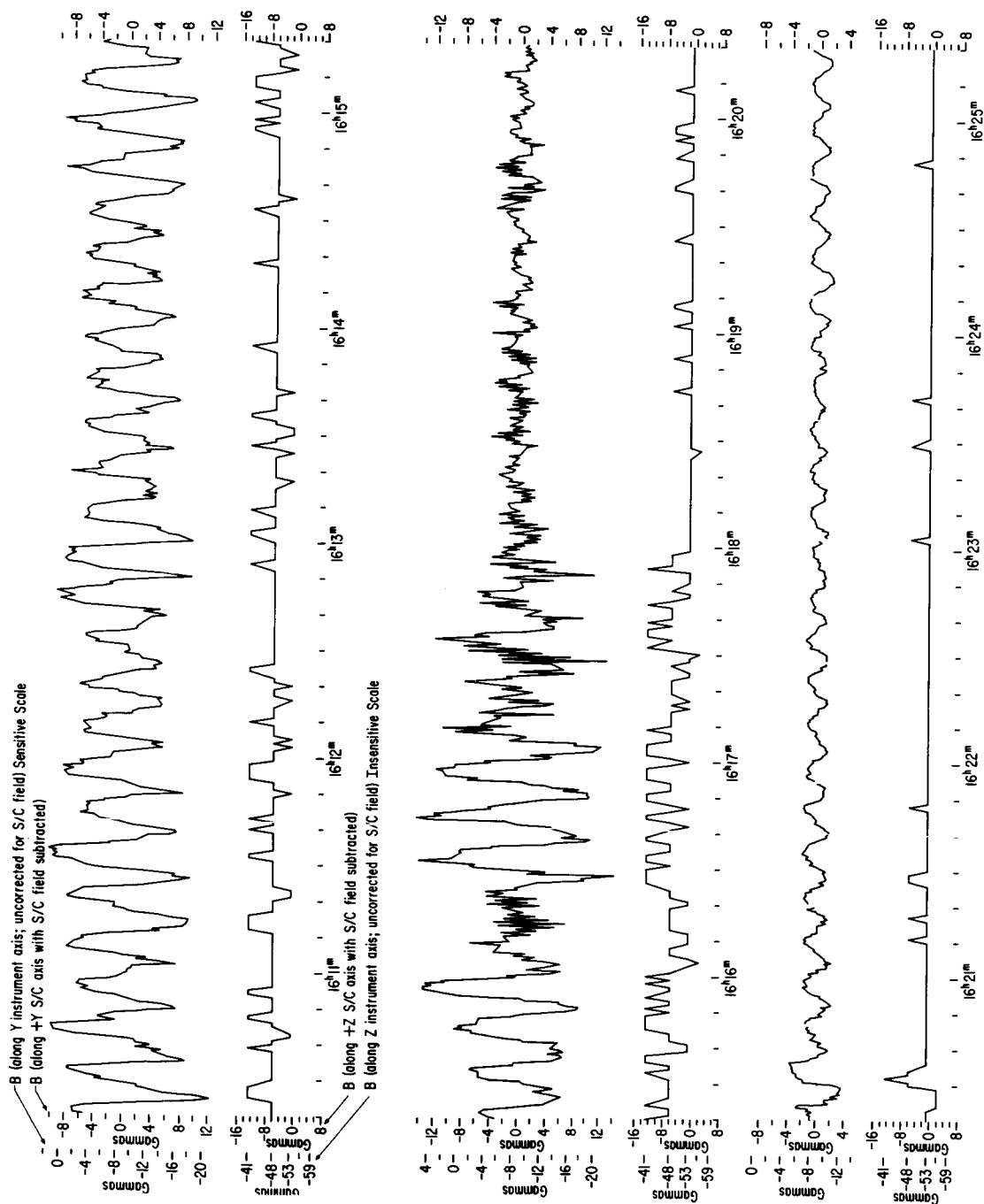


Figure 7

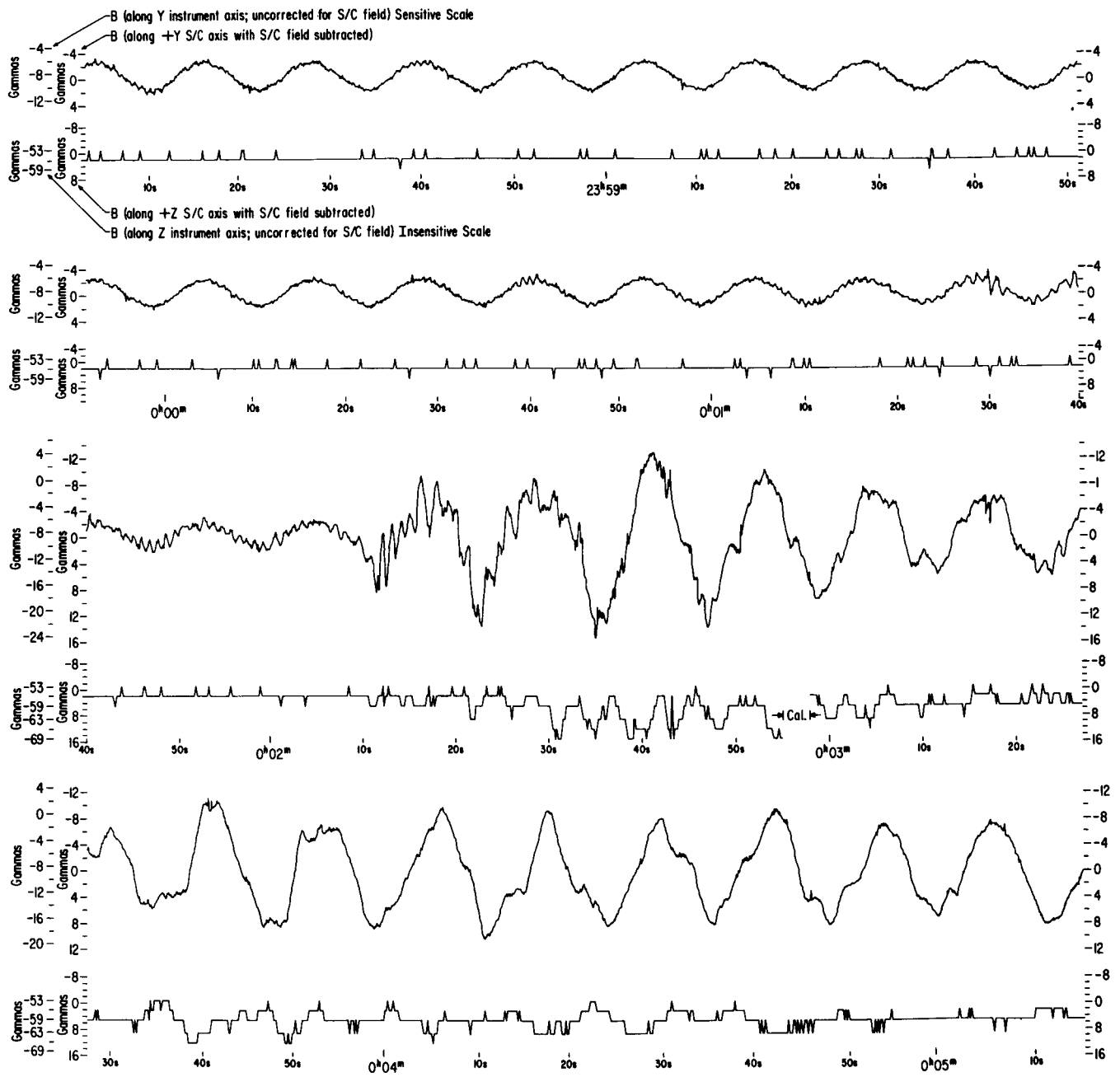


Figure 8

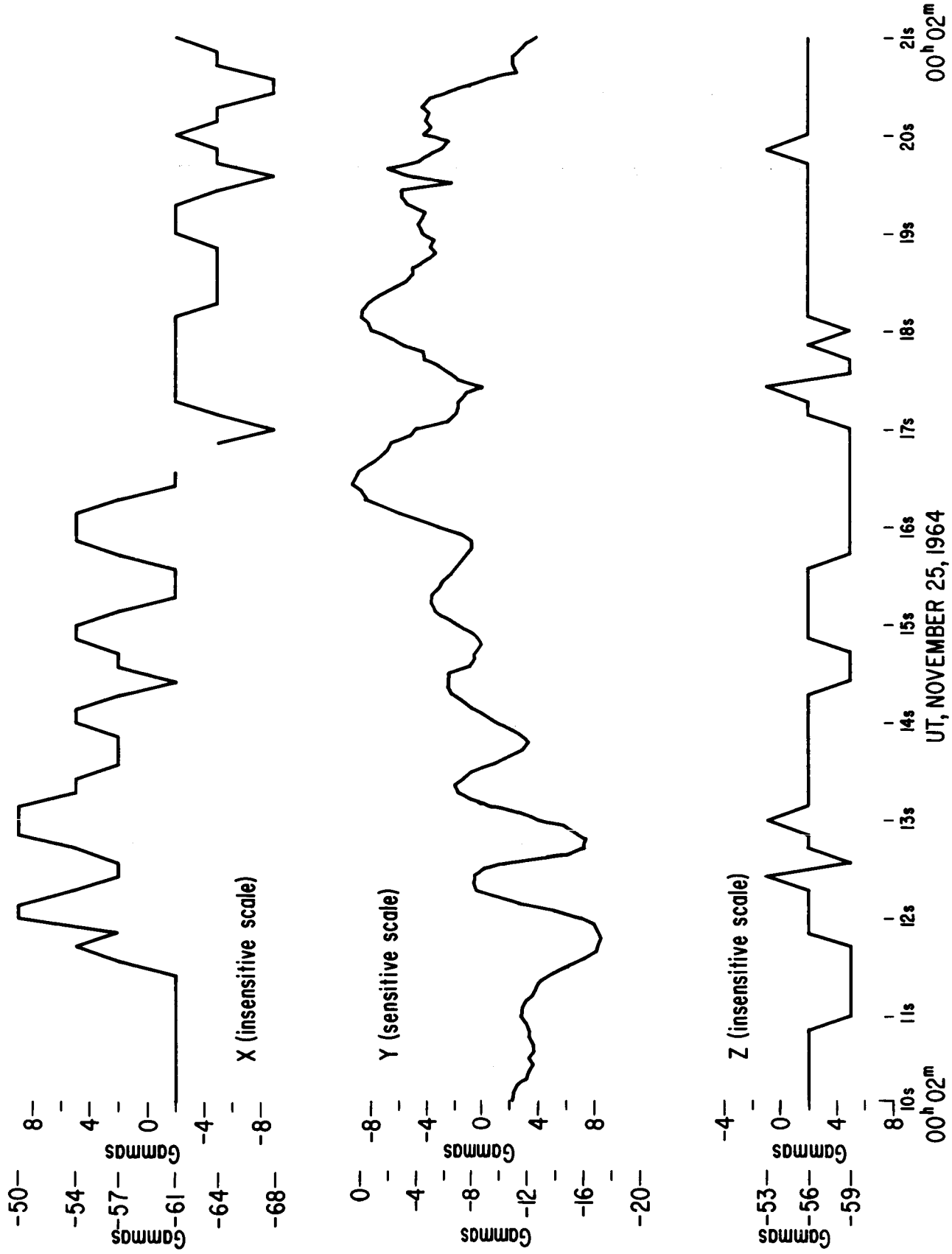
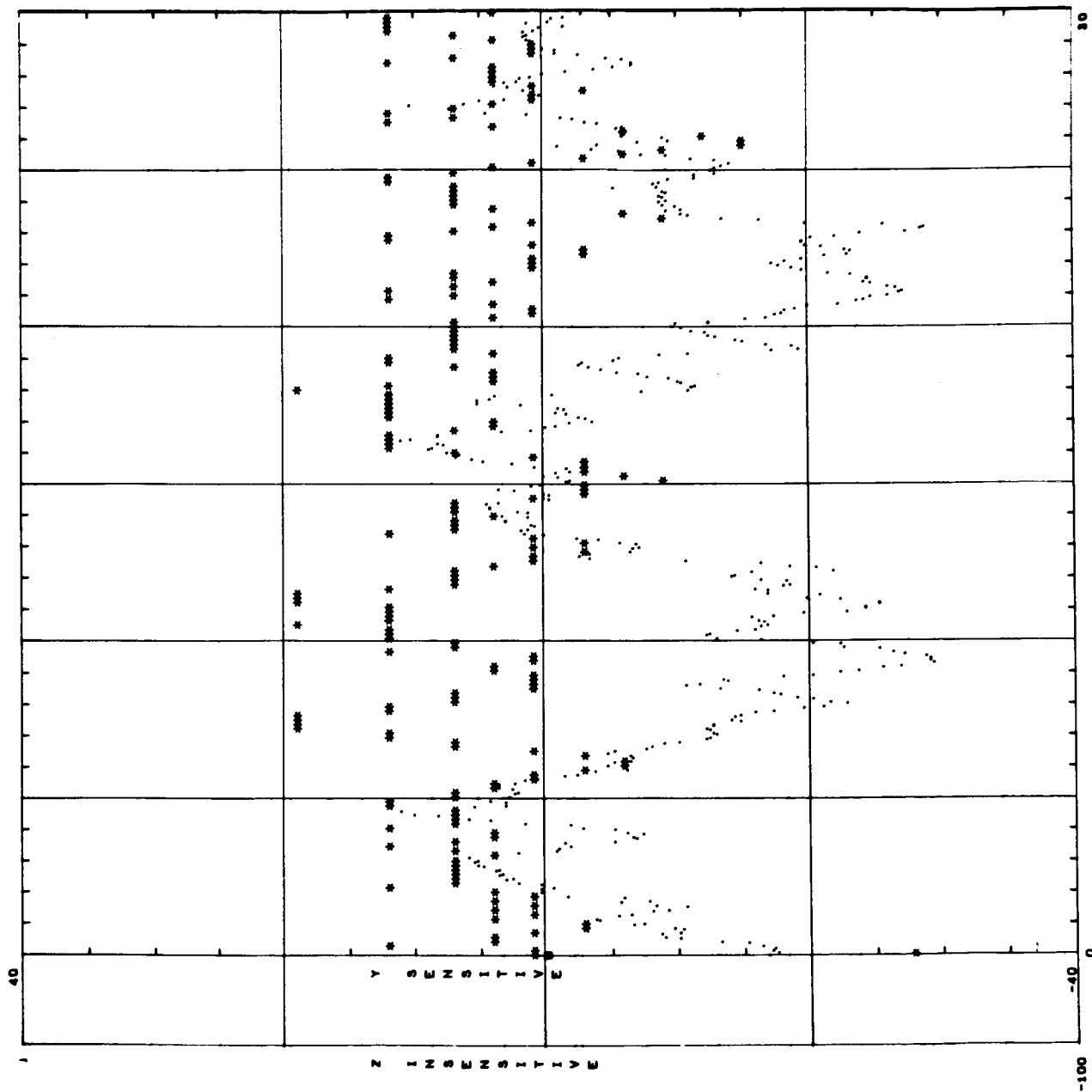


Figure 9

Y SENS IS ... 2 INSEN IS \*\*\* START TIME IS 64/353/14/0 /31



SECONDS OF TIME  
Figure 10

Y SENS IS ... 2 INSEN IS \*\*\* START TIME IS 64/353/14/0 /1

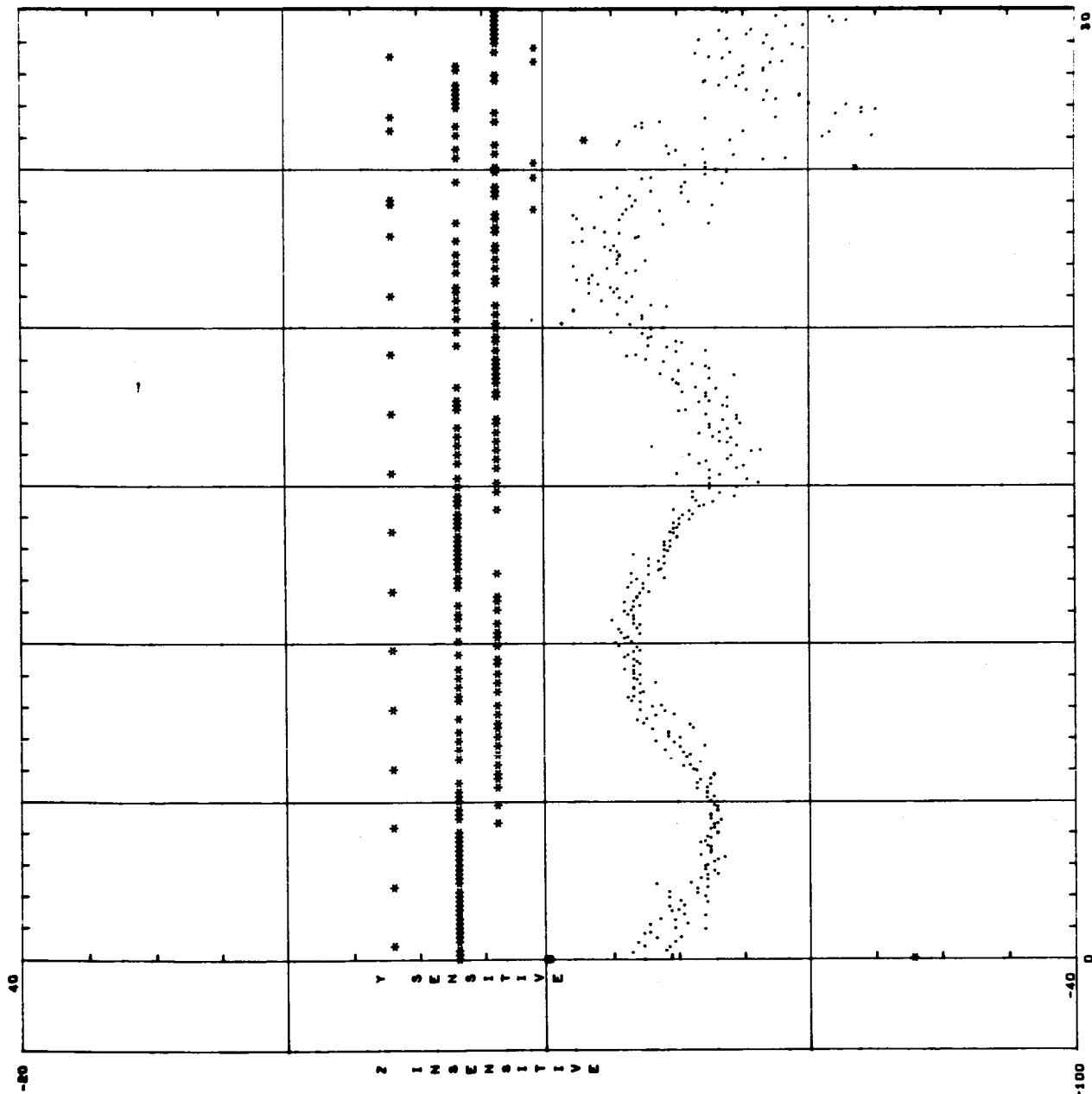


Figure 11



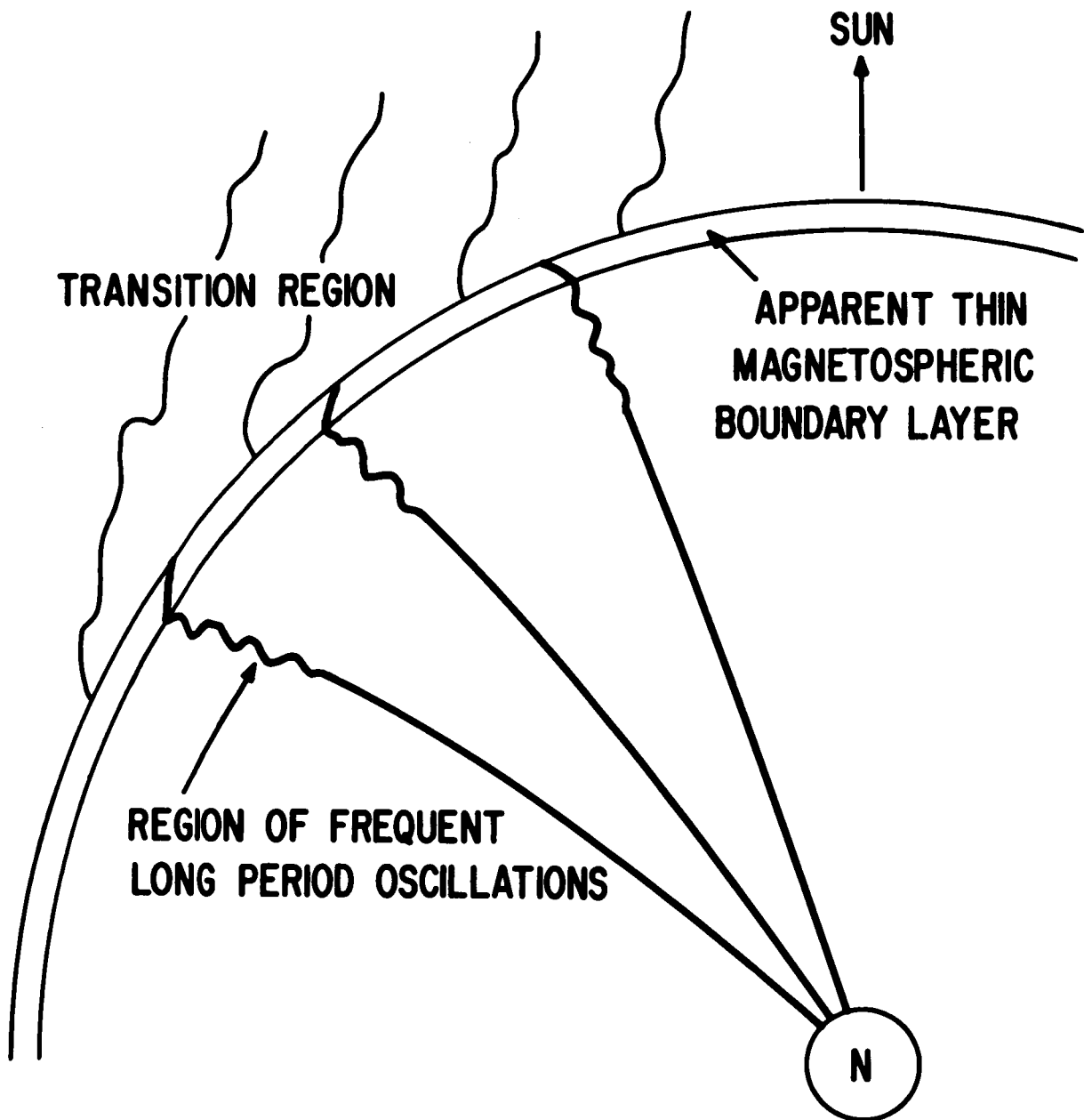
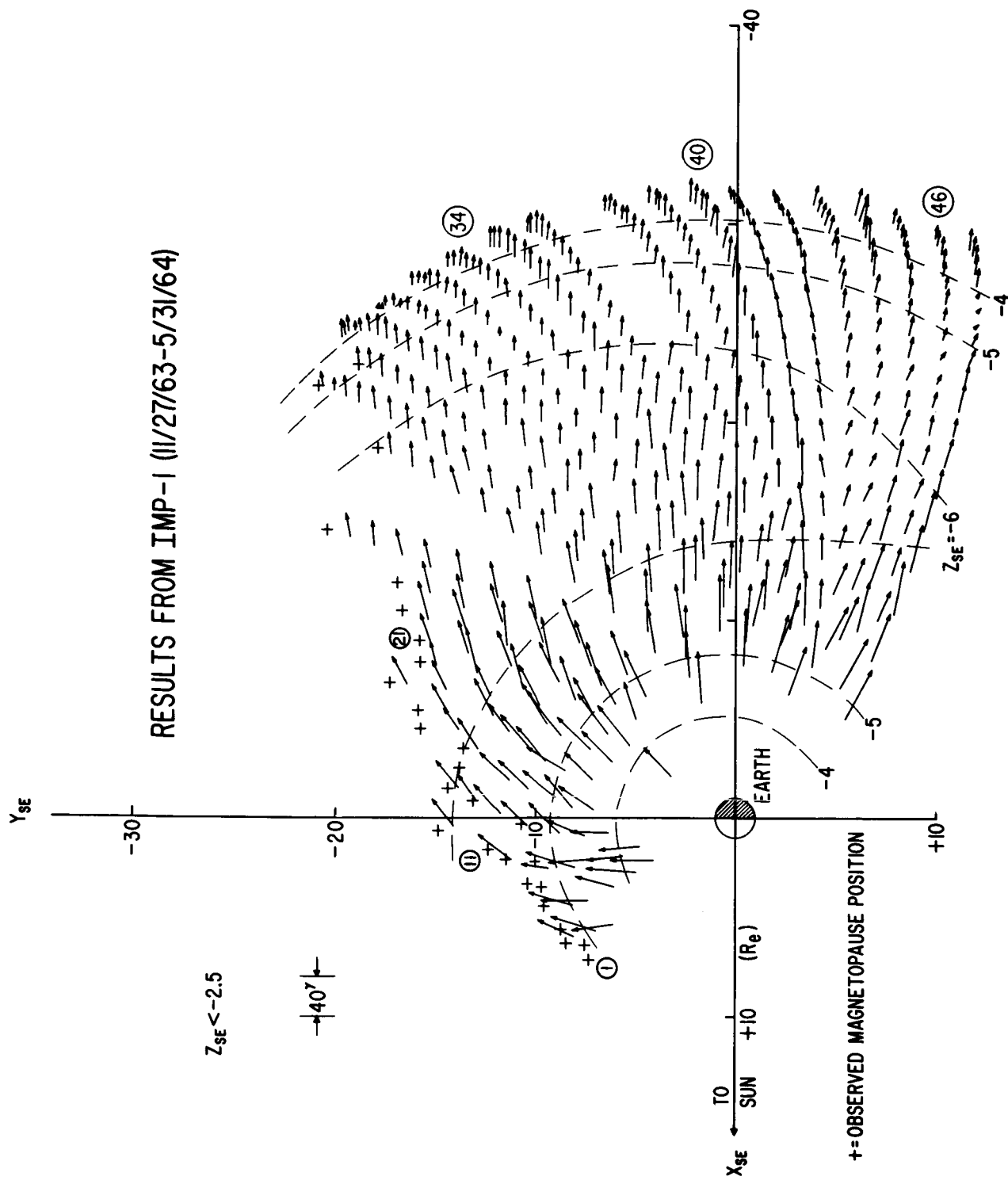


Figure 12



$X_{SE}-Y_{SE}$  COMPONENT OF MAGNETOSPHERE FIELD

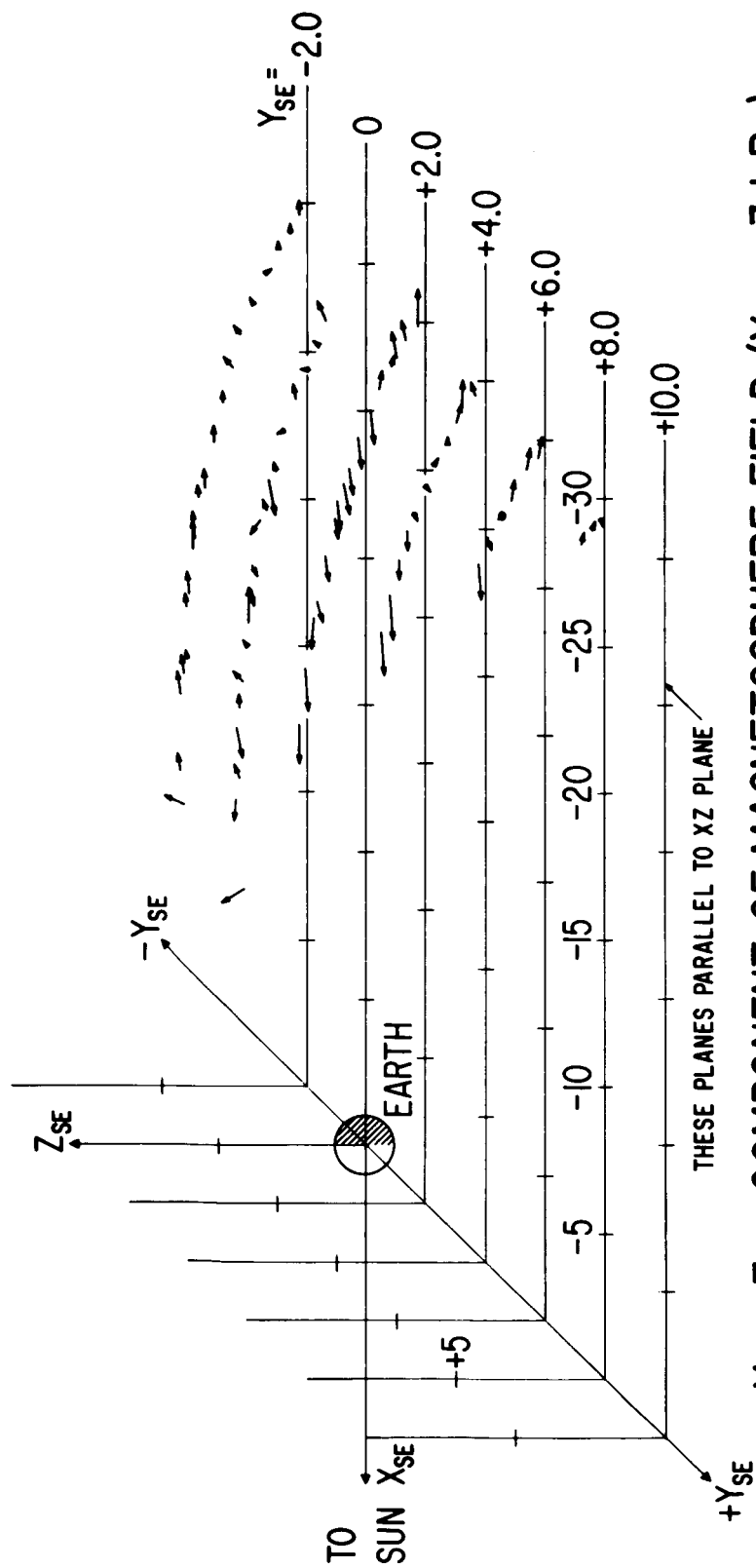
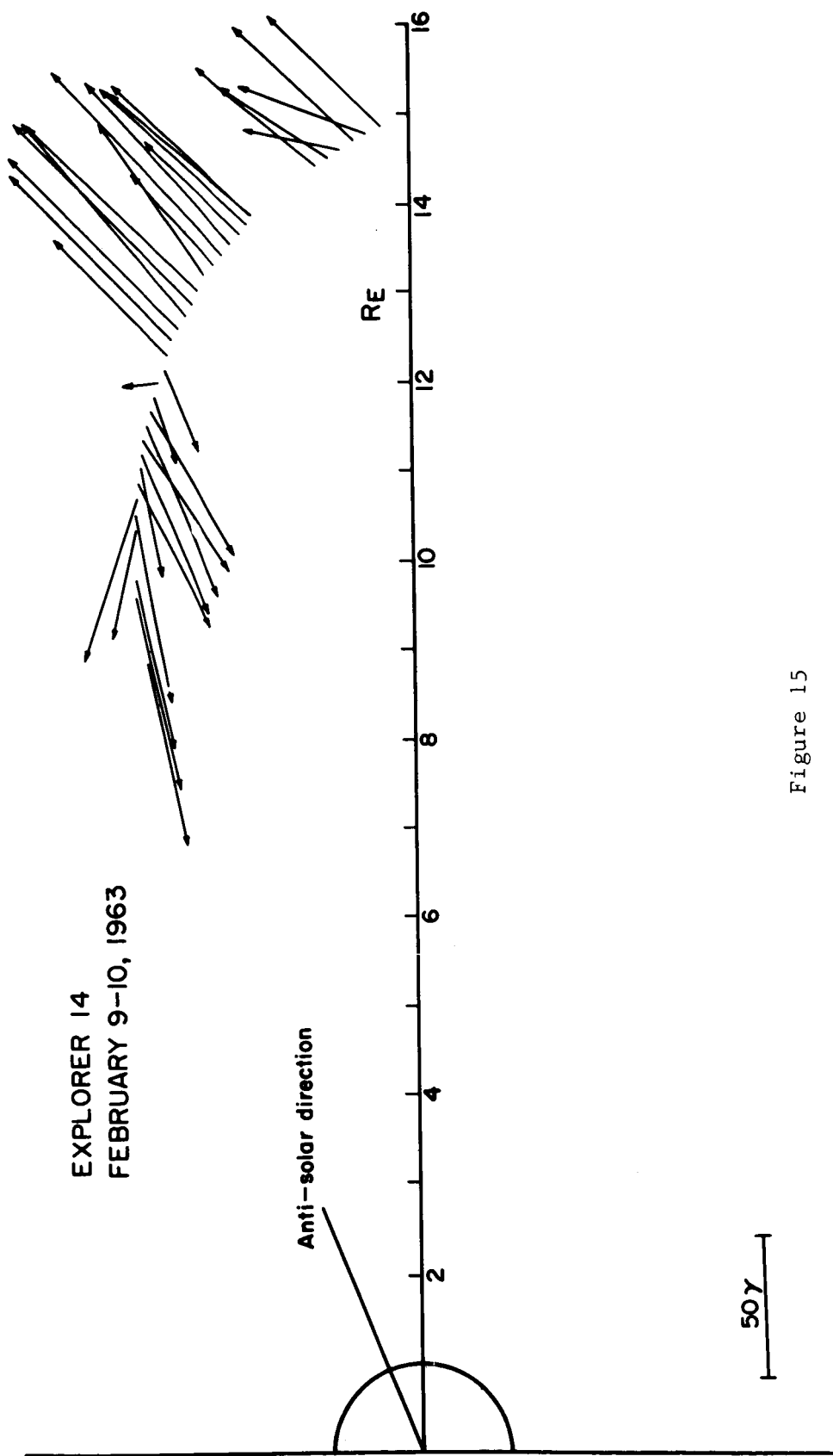


Figure 14



EXPLORER 14  
FEBRUARY 9-10, 1963

Figure 15

EXPLORER 14  
FEBRUARY 20, 1963

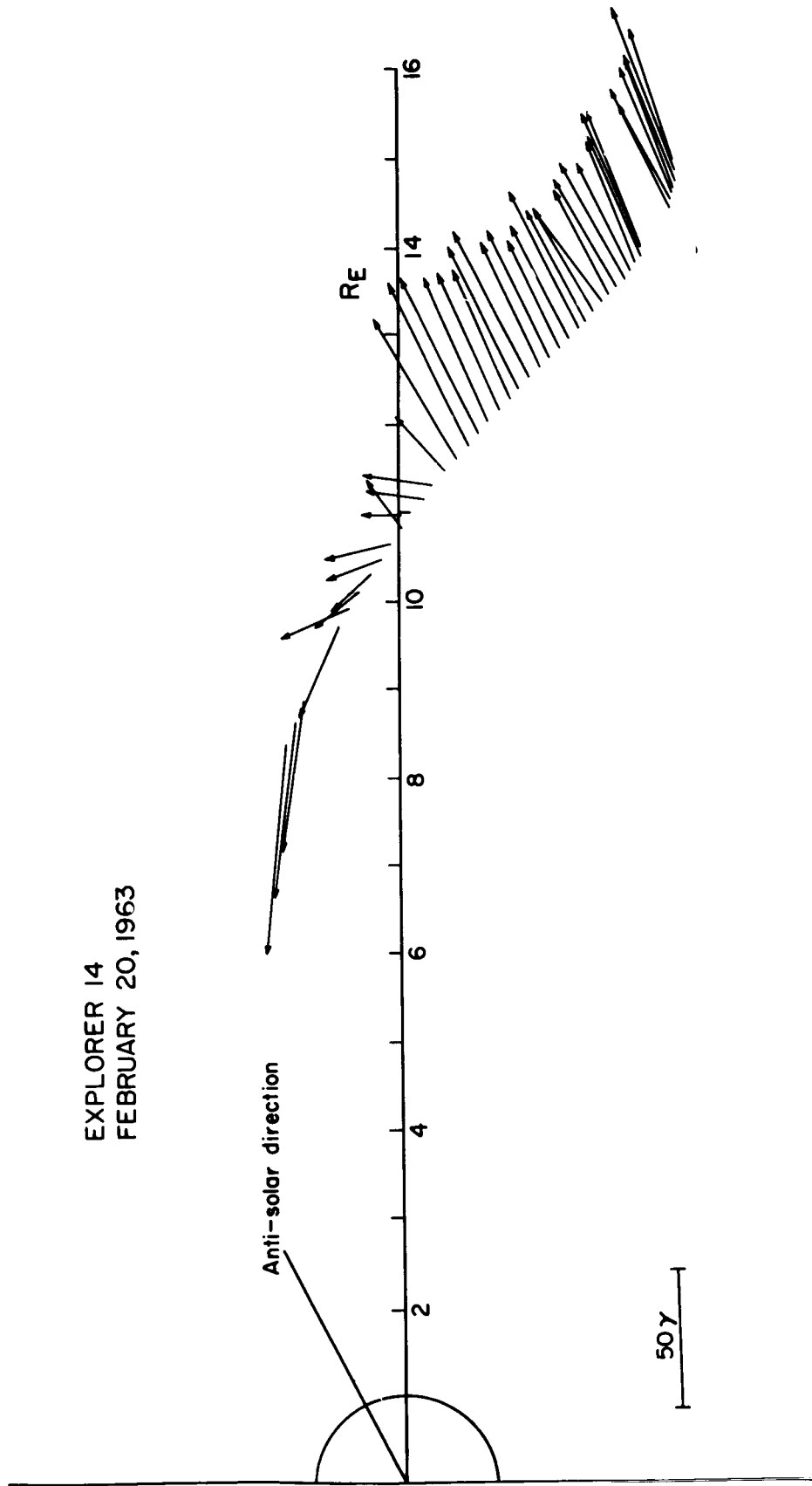


Figure 16

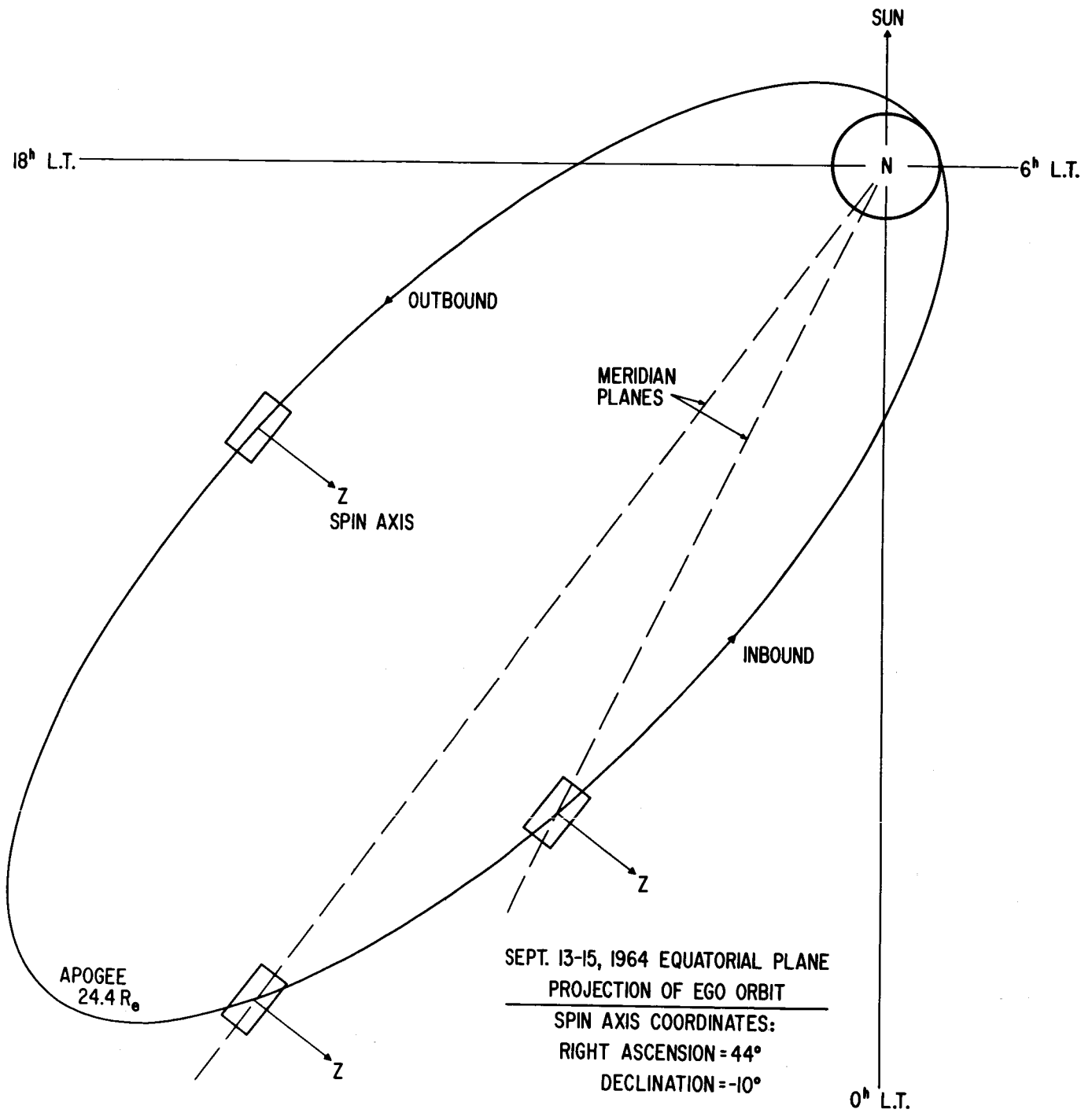


Figure 17

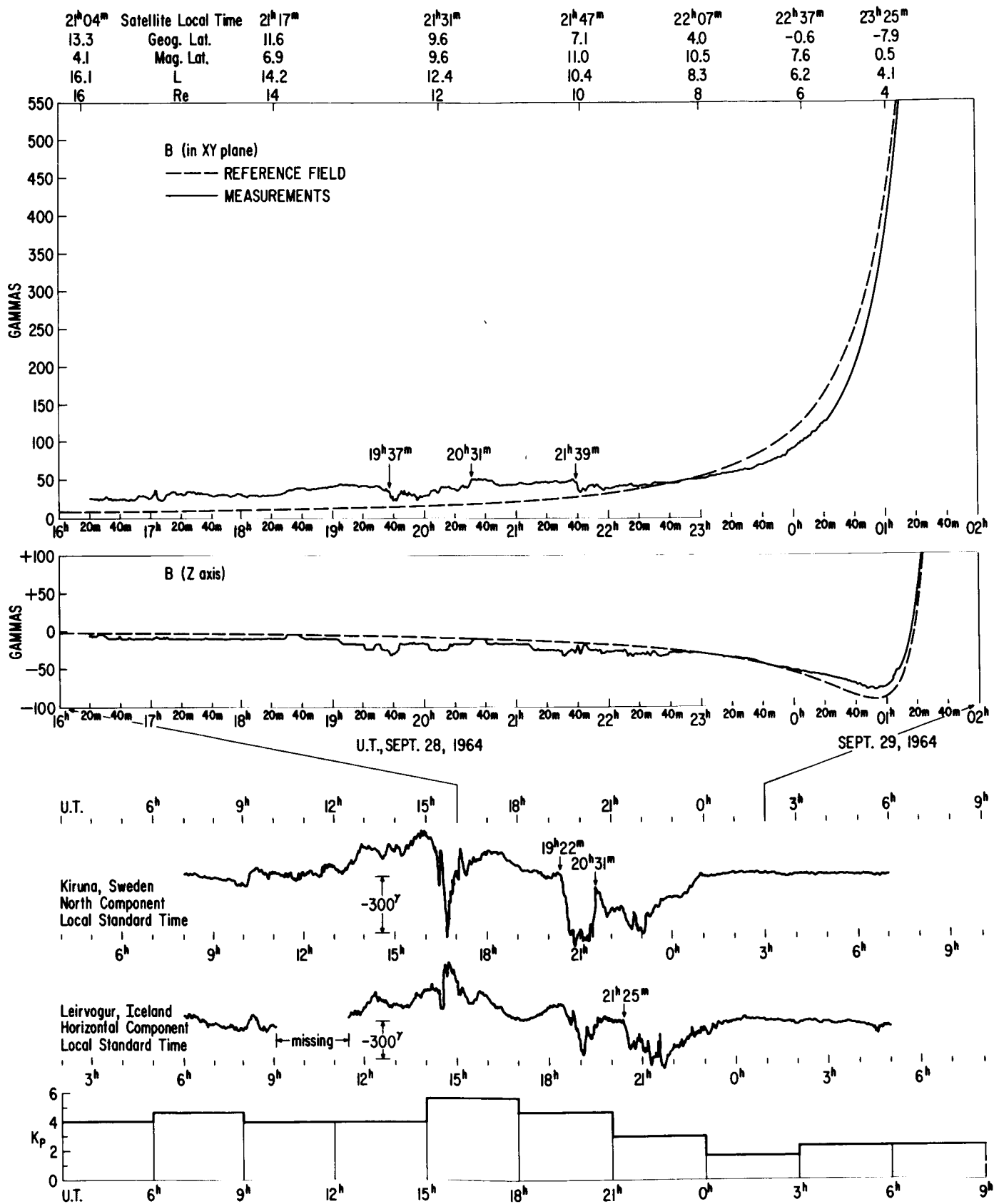


Figure 18

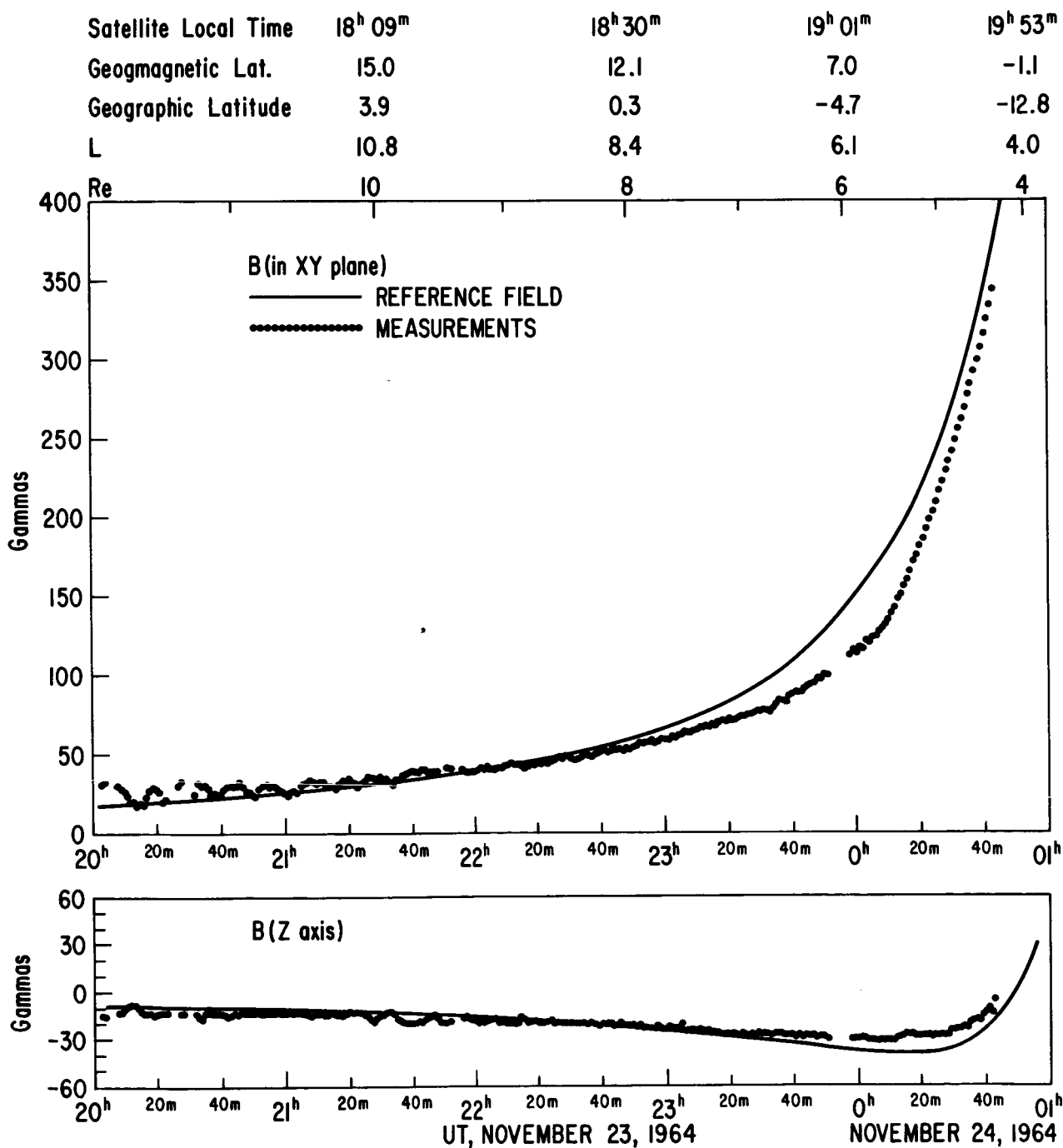


Figure 19



# During a Magnetic Disturbance

<u>Earth's Surface</u>	<u>Satellite</u>	<u>Energy Transfer</u>
Disturbance starts (Kp index increases more rapidly than Dst)	(a) Magnetospheric compression increases (b) Tail field* increases	From solar wind to outer magnetosphere
**Magnetic bays (auroral zone)	Tail field* decreases with each negative bay activation. Then increases as bay decays. (in longitude sectors of surface bay activity)	From outer magnetosphere to auroral ionosphere and possibly the inner magnetosphere ring current.
Disturbance decays (Dst decreases more slowly than Kp)	Tail field* decreases	To upper atmosphere?

\* refers to tail field at latitudes displaced from the anti-solar direction  
 \*\* occur intermittently throughout the disturbance

Figure 20

Satellite	Local Time	14 <sup>h</sup> 08 <sup>m</sup>	15 <sup>h</sup> 04 <sup>m</sup>	15 <sup>h</sup> 43 <sup>m</sup>	16 <sup>h</sup> 12 <sup>m</sup>	16 <sup>h</sup> 34 <sup>m</sup>	16 <sup>h</sup> 53 <sup>m</sup>	17 <sup>h</sup> 08 <sup>m</sup>	17 <sup>h</sup> 21 <sup>m</sup>
Mag. Lat.		23.0	24.2	24.5	24.7	24.9	25.3	25.9	26.7
L		3.5	4.8	6.0	7.3	8.5	9.8	11.1	12.5
Re		3	4	5	6	7	8	9	10

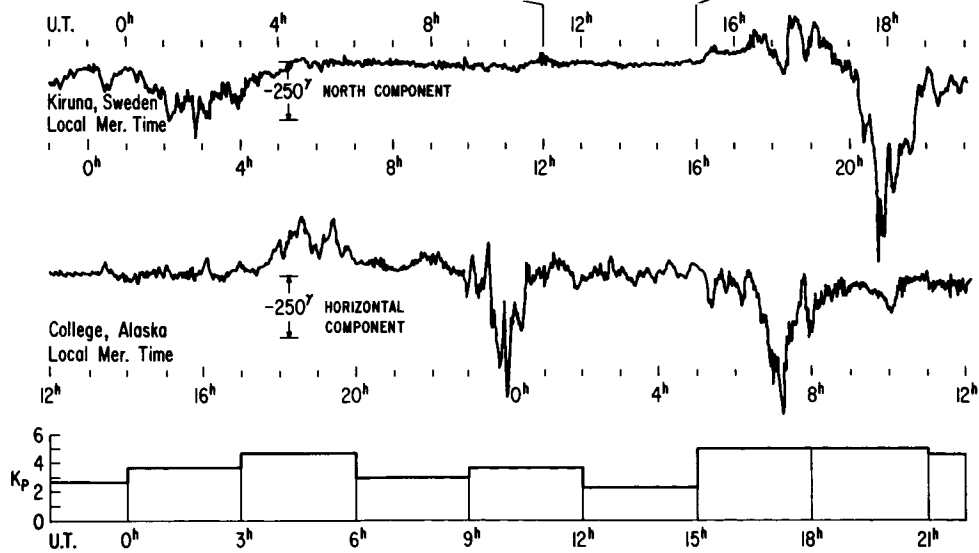
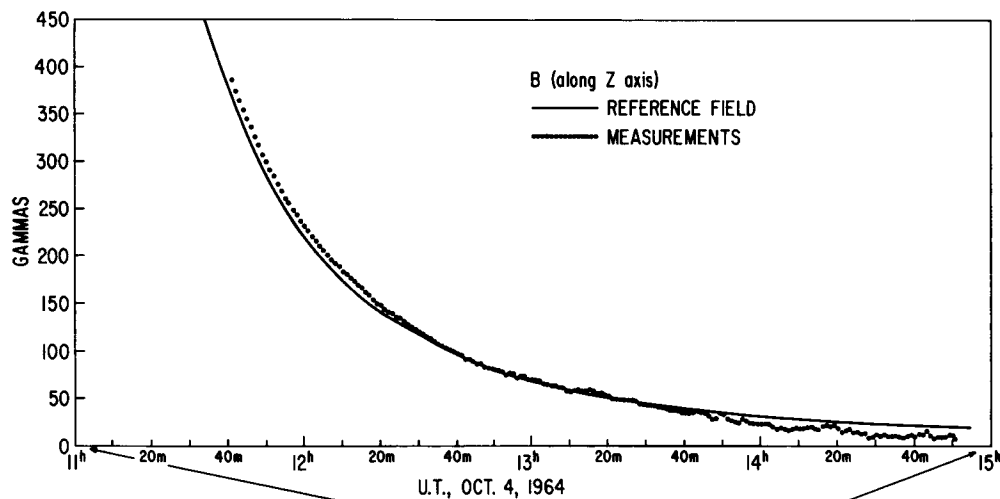
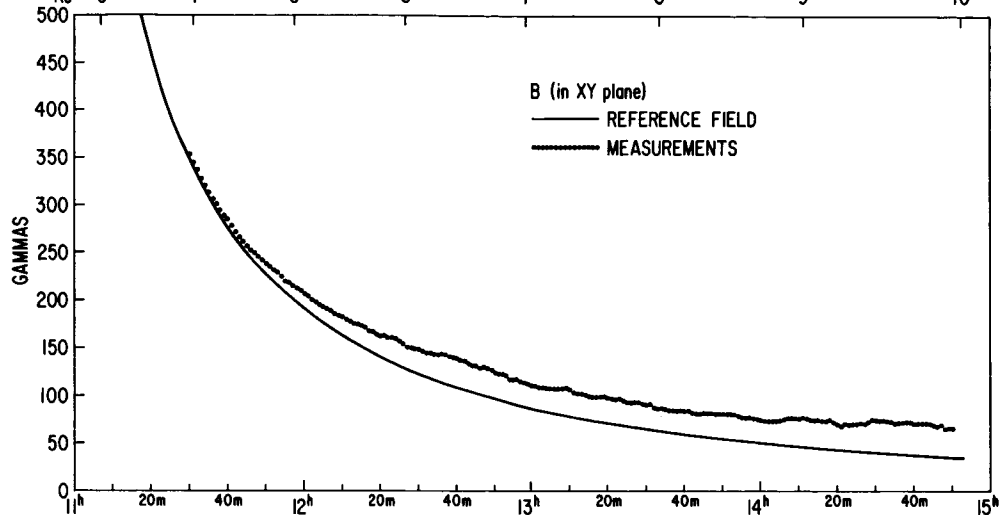


Figure 21

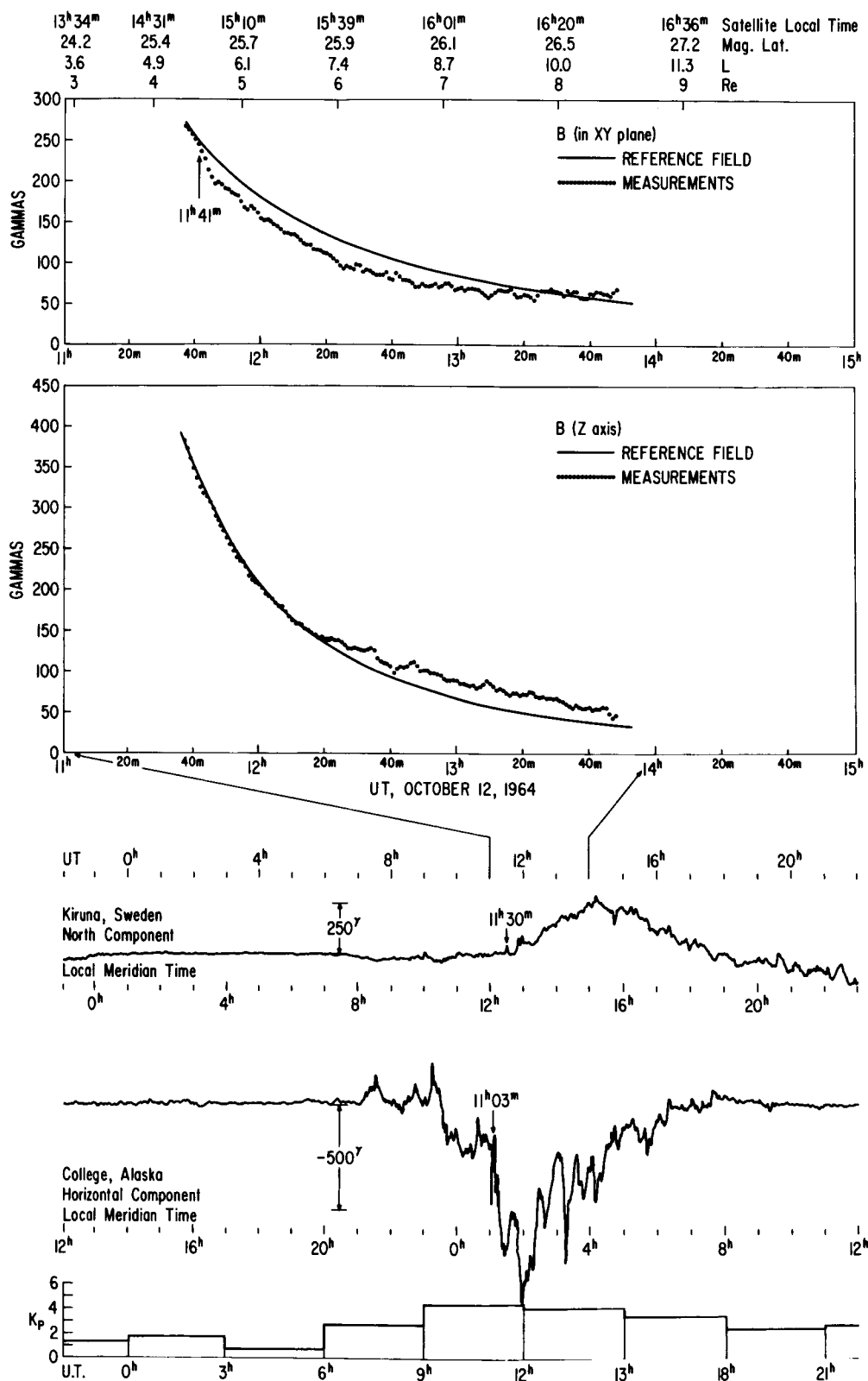


Figure 22

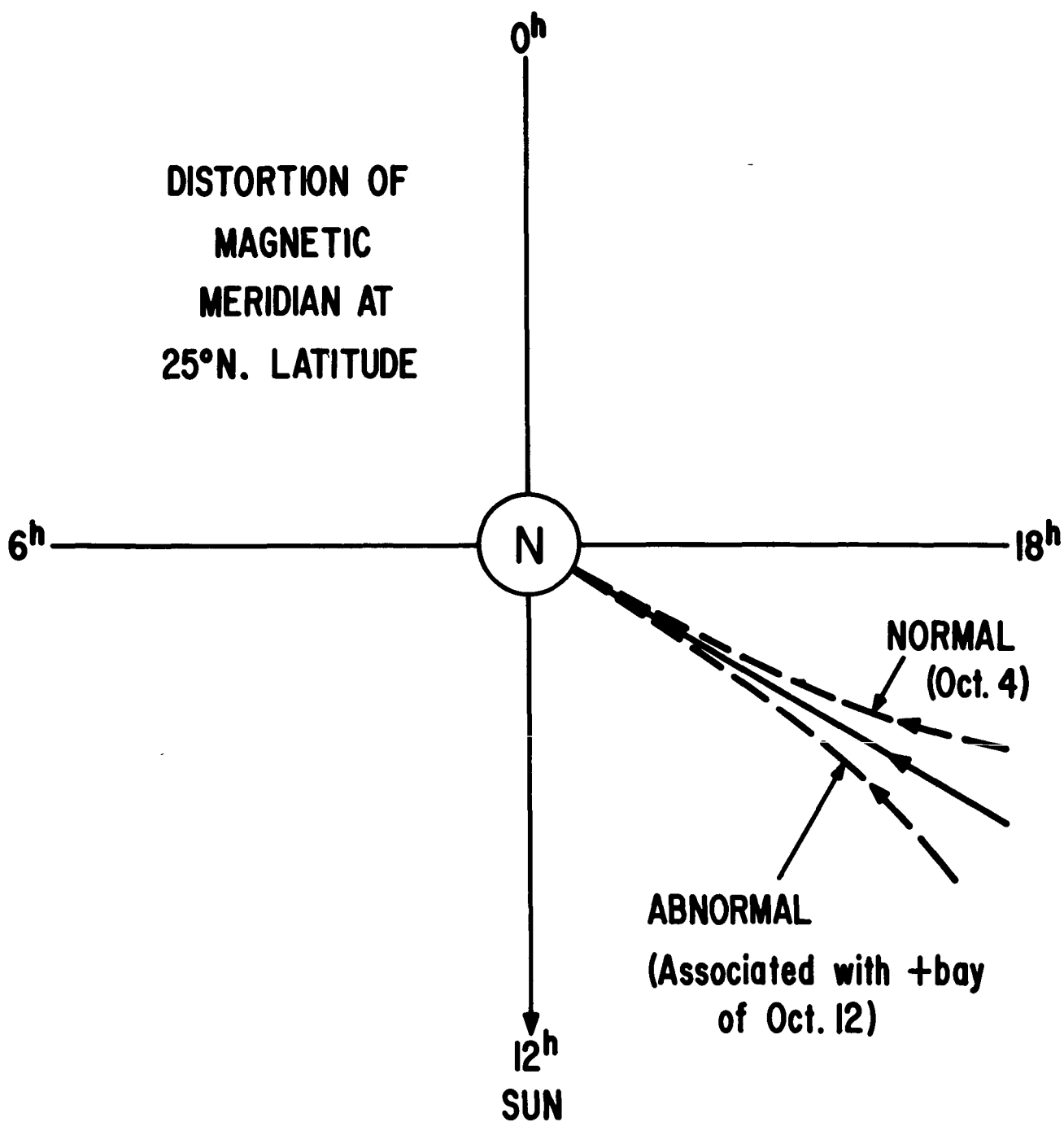


Figure 23